JOURNAL OF VIROLOGY, Nov. 2003, p. 12252–12265 Vol. 77, No. 22
0022-538X/03/$08.00+0 DOI: 10.1128/JVI.77.22.12252–12265.2003

Gamma Interferon Is Critical for Neuronal Viral Clearance and Protection in a Susceptible Mouse Strain following Early Intracranial Theiler's Murine Encephalomyelitis Virus Infection

Moses Rodriguez,[1,2]* Laurie J. Zoecklein,[1] Charles L. Howe,[2] Kevin D. Pavelko,[1] Jeff D. Gamez,[1] Shunya Nakane,[2] and Louisa M. Papke[1]

Departments of Immunology[1] and Neurology,[2] Mayo Clinic, Rochester, Minnesota 55905

Received 15 April 2003/Accepted 12 August 2003

We evaluated the role of gamma interferon (IFN-γ) in protecting neurons from virus-induced injury following central nervous system infection. IFN-$\gamma^{-/-}$ and IFN-$\gamma^{+/+}$ mice of the resistant major histocompatibility complex (MHC) *H-2^b* haplotype and intracerebrally infected with Theiler's murine encephalomyelitis virus (TMEV) cleared virus infection from anterior horn cell neurons. IFN-$\gamma^{+/+}$ *H-2^b* mice also cleared virus from the spinal cord white matter, whereas IFN-$\gamma^{-/-}$ *H-2^b* mice developed viral persistence in glial cells of the white matter and exhibited associated spinal cord demyelination. In contrast, infection of IFN-$\gamma^{-/-}$ mice of the susceptible *H-2^q* haplotype resulted in frequent deaths and severe neurologic deficits within 16 days of infection compared to the results obtained for controls. Morphologic analysis demonstrated severe injury to spinal cord neurons in IFN-$\gamma^{-/-}$ *H-2^q* mice during early infection. More virus RNA was detected in the brain and spinal cord of IFN-$\gamma^{-/-}$ *H-2^q* mice than in those of control mice at 14 and 21 days after TMEV infection. Virus antigen was localized predominantly to anterior horn cells in infected IFN-$\gamma^{-/-}$ *H-2^q* mice. IFN-γ deletion did not affect the humoral response directed against the virus. However, the level of expression of CD4, CD8, class I MHC, or class II MHC in the central nervous system of IFN-$\gamma^{-/-}$ *H-2^q* mice was lower than those in IFN-$\gamma^{+/+}$ *H-2^q* mice. Finally, in vitro analysis of virus-induced death in NSC34 cells and spinal motor neurons showed that IFN-γ exerted a neuroprotective effect in the absence of other aspects of the immune response. These data support the hypothesis that IFN-γ plays a critical role in protecting spinal cord neurons from persistent infection and death.

A major area of investigation in neurovirology is directed toward understanding the factors that participate in neuronal viral clearance versus viral persistence. Clearance of virus from the infected central nervous system (CNS) is unique because of the intact blood-brain barrier, the relative absence of major histocompatibility complex (MHC) molecules on neuronal cells, and the lack of well-established lymphatic drainage. Nevertheless, once viruses replicate in the CNS, there is a vigorous immune response directed toward the clearance of virus antigen from infected cells. Antibody plays a critical role in neutralizing extracellular viral particles and also has been proposed to participate in the clearance of intracellular virus (4, 21). However, the manner in which antibody enters cells or interacts with surface cellular receptors to prevent viral persistence in neurons is not well understood.

The classical way in which intracellular virus is eliminated is by cytotoxic T cells that are restricted by class I MHC. The control of MHC expression on neurons is dependent upon electrical activity (36). Neurons with normal electrical activity suppress MHC expression, whereas silent or injured neurons up-regulate class I MHC expression, an activity that makes them susceptible to class I MHC-mediated injury. Disruption of electrical activity induces class II MHC expression on microglia and astrocytes (36). Following virus infection in the CNS, class I MHC is rapidly up-regulated (1, 26) in neuronal cells. In particular, soluble factors such as alpha/beta interferon (IFN-α/β) (39) are required for the up-regulation of MHC in most CNS cells, including neurons. Cytotoxic T-cell responses in brain infiltrating mononuclear inflammatory cells have been demonstrated (23, 24, 25, 28) and have been shown to participate in viral clearance. However, the consequences to the CNS are a "double-edged sword." Virus is cleared at the expense of the destruction of neurons that are not renewable and whose death results in permanent functional deficits. For example, cytotoxic T cells have been shown to transect neurites expressing class I MHC (31). Therefore, this vigorous cytotoxic response may participate directly in immune-mediated pathology.

However, there are examples where viruses are cleared from the CNS without significant destruction of brain parenchyma (2). In these situations, the hypothesis proposed is that factors secreted by cytotoxic lymphocytes participate in viral clearance without cytotoxicity. Of the factors that are secreted by immune cells and that are thought to play a critical role in viral clearance, IFN-γ has received the most attention (33). IFN-γ is a 50-kDa N-glycosylated noncovalent homodimer composed of two identical 17-kDa polypeptides. It is produced by activated NK cells and T cells. IFN-γ induces many immunomodulatory effects on CNS cells, including activation of macrophages, promotion of leukocyte adhesion to allow trafficking of cells to the

* Corresponding author. Mailing address: Department of Immunology, Mayo Clinic, 200 1st St. SW, Rochester, MN 55905. Phone: (507) 284-4663. Fax: (507) 284-1637. E-mail: rodriguez.moses@mayo.edu.

CNS, direct antiviral and antiproliferative effects, and induction of the release of other cytokines, including tumor necrosis factor alpha and interleukin 1. IFN-γ is one of the most potent factors up-regulating MHC expression on macrophages and microglia. In addition, IFN-γ has been implicated in the clearance of virus from CNS neurons following infection with herpes simplex virus type 1 (13), measles virus (41), retrovirus (LP-BM5) (20), and alphaviruses (2).

We examined the role of IFN-γ in a model of viral CNS infection that localizes predominantly to neurons early in the course of disease. Intracerebral injection of Theiler's murine encephalomyelitis virus (TMEV), a picornavirus, induces a characteristic disease in the CNS of mice (29). During the first 10 to 12 days of infection, the virus replicates primarily in neurons of the hippocampus, striatum, and cortex in the brain and in the anterior horn of the spinal cord; then is rapidly cleared from the CNS (10), irrespective of MHC haplotype. Oligodendrocytes and macrophages are also infected early (38). In mice of resistant MHC haplotypes *H-2*^{b}, *H-2*^{d}, and *H-2*^{k}, no demyelination or viral persistence develops. In animals of susceptible MHC haplotypes *H-2*^{s}, *H-2*^{v}, *H-2*^{r}, *H-2*^{u}, *H-2*^{f}, and *H-2*^{q}, the virus persists in glial cells (44) and macrophages (6, 22, 52), in particular, in the spinal cord white matter and brain stem.

In order to examine the role of IFN-γ in TMEV-induced neuronal injury, we used mice with a specific disruption in the IFN-γ gene. The original IFN-γ$^{-/-}$ mice were generated in a B6/129 background (MHC haplotype *H-2*^{b}) that is resistant to TMEV persistence and subsequent demyelination. Murray et al. showed previously that resistance was inhibited in IFN-γ$^{-/-}$ *H-2*^{b} mice and that these mice developed chronic myelin injury associated with viral persistence in the spinal cord white matter (35). To address the contribution of IFN-γ in mice of a susceptible haplotype, we generated a line of IFN-γ$^{-/-}$ mice with MHC haplotype *H-2*^{q}. These mice exhibited markedly decreased survival and increased spinal cord pathologic changes compared to infected IFN-γ$^{+/-}$ *H-2*^{q} littermate controls and IFN-γ$^{+/+}$ *H-2*^{q} parental controls. In addition, we found that IFN-γ is critical for the prevention of lethal infection of anterior horn motor neurons in vivo in mice of the *H-2*^{q} haplotype and is able to protect NSC34 motor neurons and primary spinal motor neurons from virus-induced cell death in vitro. These data support the hypothesis that IFN-γ not only is necessary for the clearance of picornavirus infection from CNS neurons in mice of a susceptible haplotype but also is necessary for the protection of neurons from virus-associated death.

MATERIALS AND METHODS

Virus. The Daniels strain of TMEV (DAV) was used for all experiments (29).

Mice. Mice were obtained from Jackson Laboratories (Bar Harbor, Maine). C57BL/6-*Ifng*^{tm1Ts} mice have a targeted disruption of the IFN-γ gene and are homozygous for MHC class I *H-2*^{b}; C57BL/6 mice served as controls in all experiments used to evaluate the resistant *H-2*^{b} haplotype. IFN-γ$^{-/-}$ *H-2*^{q} mice were generated by backcrossing IFN-γ knockout mice to B10.D1-H2^q/SgJ (IFN-γ$^{+/+}$ *H-2*^{q}) mice from Jackson Laboratories. F_1 mice were mated to obtain F_2 breeding pairs negative for the wild-type IFN-γ gene and *H-2*^{b}. Mice were screened by PCR. The normal endogenous IFN-γ gene was detected with forward primer IMR126 (5′-AGA AGT AAG TGG AAG GGC CCA GAA G-3′) and downstream primer IMR127 (5′-AGG GAA ACT GGG AGA GGA GAA ATA T-3′). This process resulted in a 220-bp product for mice with normal expression of IFN-γ. The targeted IFN-γ allele was detected with forward primer IMR128 (5′-TCA GCG CAG GGG CGC CCG GTT CTT T-3′) and downstream primer IMR129 (5′-ATC GAC AAG ACC GGC TTC CAT CCG A-3′). This process resulted in a 375-bp product for IFN-γ$^{-/-}$ mice. Mice that were positive for both alleles indicated heterozygosity. IFN-γ$^{-/-}$ mice were further screened by fluorescence-activated cell sorting with an antibody to *H-2*^{b} (BD Pharmingen, San Diego, Calif.). Mice that were negative for *H-2*^{b} were used as breeders to establish the *H-2*^{q} line of mice. All offspring were screened by both assays to confirm genotype. IFN-γ$^{+/-}$ *H-2*^{q} mice were generated by crossing IFN-γ$^{+/+}$ *H-2*^{q} mice to IFN-γ$^{-/-}$ *H-2*^{q} mice. All comparisons to IFN-γ$^{-/-}$ *H-2*^{q} mice were performed with IFN-γ$^{+/-}$ *H-2*^{q} mice or IFN-γ$^{+/+}$ *H-2*^{q} mice.

Infection and harvesting of the CNS for morphologic analysis. At 4 to 6 weeks of age, mice were infected intracerebrally with 2×10^5 PFU of TMEV in a total volume of 10 μl. At various times after infection (or when moribund), mice were perfused via intracardiac puncture with 50 ml of Trump's fixative. Spinal cords and brains were removed and postfixed in Trump's fixative for 24 to 48 h in preparation for morphologic analysis.

Spinal cord morphometry. Spinal cords were removed from spinal columns and cut into 1-mm coronal blocks. Every third block was treated with osmium tetroxide and embedded in glycol methacrylate (46, 48, 49). Sections of 2 μm were prepared and stained with a modified Erichrome-cresyl violet stain (43). Morphologic analysis was performed on 12 to 15 sections per mouse as previously described (46, 48, 49). Briefly, each quadrant of every coronal section from each mouse was graded for the presence or absence of gray matter disease, meningeal inflammation, and demyelination. The score was expressed as the percentage of spinal cord quadrants examined with the pathologic abnormality. A maximum score of 100 indicated that there was a particular pathologic abnormality in every quadrant of all spinal cord sections from a given mouse. All grading was performed without knowledge of the experimental group. Additional spinal cord blocks were embedded in paraffin for immunocytochemical analysis.

Brain pathologic changes. Brain pathologic changes were assessed at 7, 11 to 16, and 21 days postinfection (p.i.) by using a previously described technique (10). Following perfusion with Trump's fixative, two coronal cuts were made in the intact brain at the time of removal from the skull (one section through the optic chiasm and another section through the infundibulum). As a guide, we used the *Atlas of the Mouse Brain and Spinal Cord* (sections 220 and 350) (53). The three blocks obtained were embedded in paraffin. The resulting slides were stained with hematoxylin and eosin. This procedure allowed for systematic analysis of the pathologic changs in the cortex, corpus callosum, hippocampus, brain stem, striatum, and cerebellum.

Pathologic scores were assigned without knowledge of the experimental group to the following areas of the brain: cortex, corpus callosum, hippocampus, brain stem, striatum, and cerebellum. Each area of the brain was graded on a 4-point scale as follows: 0, no pathologic changes; 1, no tissue destruction and only minimal inflammation; 2, early tissue destruction (loss of architecture) and moderate inflammation; 3, definite tissue destruction (demyelination, parenchymal damage, cell death, neurophagia, and neuronal vacuolation); and 4, necrosis (complete loss of all tissue elements, with associated cellular debris). Meningeal inflammation was assessed and graded as follows: 0, no inflammation; 1, one cell layer of inflammation; 2, two cell layers of inflammation; 3, three cell layers of inflammation; and 4, four or more cell layers of inflammation. The area with the maximal extent of tissue damage was used for the assessment of each brain region.

Survival analysis. Mice were monitored throughout the period of infection, and deaths were recorded at the end of each week.

Virus-specific antibody isotype ELISA. Whole blood was collected from mice at the time of sacrifice, and sera were isolated and stored at −80°C. Levels of total serum immunoglobulin G (IgG) and IgM against TMEV were assessed by using an enzyme-linked immunosorbent assay (ELISA) as previously described (37). Purified virus was allowed to adsorb to 96-well plates (Immulon II; Dynatech Laboratories Inc., Chantilly, Va.) and then was blocked with 1% bovine serum albumin (Sigma Chemical Co., St. Louis, Mo.) in phosphate-buffered saline (PBS). Serial serum dilutions were made with 0.2% bovine serum albumin-PBS and were added in triplicate. Biotinylated anti-mouse IgG or IgM secondary antibodies were used for detection (Jackson Immunoresearch Labs, Westbury, N.Y.). Signals were amplified with streptavidin-labeled alkaline phosphatase (Jackson Immunoresearch Labs) and detected with *p*-nitrophenyl phosphate as the substrate. Absorbances were read at 405 nm and plotted against serum dilution factors.

Virus neutralization assays. Virus-neutralizing antibodies were assessed as previously described (51). Briefly, TMEV was diluted to contain 50 PFU per sample and then was mixed with equal volumes of serial twofold dilutions of heat-inactivated sera from infected mice. Following incubation at 25°C for 1 h, this mixture was assayed for infectivity by plaque assays with L2 cells.

Immunostaining for virus antigen. Immunocytochemical analysis was performed with paraffin-embedded sections as previously described (9). Slides were deparaffinized in xylene and rehydrated through an ethanol series (absolute and 95, 70, 50, and 30%). Virus antigen staining was carried out with polyclonal antisera to strain DAV (50), which react strongly with the capsid proteins of TMEV. Following incubation with biotinylated secondary antibodies (Vector Laboratories, Burlingame, Calif.), immunoreactivity was detected by using the avidin-biotin-immunoperoxidase technique (Vector Laboratories). The reaction was developed with Hanker-Yates reagent and with hydrogen peroxide as the substrate (Polysciences, Warrington, Pa.). Slides were lightly counterstained with Gill's hematoxylin. The data were expressed as the percentage of spinal cord quadrants showing virus antigen-positive cells in either the gray matter or the white matter in the spinal cord.

Immunostaining for CD4, CD8, class I MHC, class II MHC, and F4/80. Frozen sections were prepared by embedding spinal cord tissue from IFN-$\gamma^{-/-}$ and IFN-$\gamma^{+/+}$ mice in OCT embedding compound. The spinal cord was removed and prepared in three longitudinal sections. The blocks were frozen and stored in liquid nitrogen until immunostaining for CD4, CD8, class I MHC, class II MHC, and F4/80 (a marker of microglia and macrophages) was performed. Frozen sections (10-μm thick) of the spinal cord were cut and placed on Superfrost Plus slides (Fisher) and allowed to air dry. Slides were fixed in 95% ethanol at −20°C for 20 min and then washed twice with PBS for 5 min each time. Samples were blocked with avidin and biotin (Vector Laboratories) for 10 min each time, and slides were washed with PBS. Primary antibodies for CD4 and CD8 (Pharmingen) and antibodies to class I MHC (28148; Pharmingen), class II MHC (MKD6; ATCC), and F4/80 (HB-198; American Type Culture Collection) were used to identify antigens. Appropriate biotin-labeled secondary antibodies were used to detect the primary antibodies. Final detection was performed by using avidin-biotin complex methodology (Vector Laboratories) and 3,3′-diaminobenzidine tetrahydrochloride (Polysciences). Following development, slides were lightly counterstained with hemotoxylin and dehydrated, and coverslips were added.

RNA isolation. The brains and spinal cords were removed from animals infected with TMEV. Total RNA was extracted from the brains and spinal cords. Briefly, the tissues were frozen and stored in liquid nitrogen. Tissue samples were homogenized in RNA-Stat60 (1 ml/100 mg of tissue) (Tel-Test, Inc., Friendswood, Tex.) with a homogenizer, and total RNA was isolated according to the manufacturer's recommendations. RNA concentrations were determined by spectrophotometry. RNA samples were equilibrated to a concentration of 0.25 μg/μl and stored at −80°C.

RT-PCR and real-time analysis. The VP2 fragment of TMEV, a viral capsid region of DAV, was amplified by reverse transcription (RT)-PCR with gene-specific primers. The primer pair sequences for VP2 of DAV were as follows: forward, 5′-TGGTCGACTCTGTGGTTACG-3′, and reverse, 5′-GCCGGTCT TGCAAAGATAGT-3′. Glyceraldehyde-3-phosphate dehydrogenase (GAPDH) was used as a control for intersample variability. The sequences used for assaying the presence of GAPDH were as follows: forward, 5′-ACCACCATGGAGAA GGC-3′, and reverse, 5′-GGCATGGACTGTGGTCATGA-3′. The sizes of the PCR products amplified with the primers were 238 bp for VP2 and 236 bp for GAPDH.

Gene copy standards were generated with each set of samples. Standards were generated with serial 10-fold dilutions of plasmid cDNA. Standards were amplified in parallel with unknown samples by real-time quantitative RT-PCR with a LightCycler (Roche, Indianapolis, Ind.). Analysis to generate standard curves was performed with LightCycler 3 software. Negative controls (with input cDNA omitted) were also used in each PCR run to confirm the specificity of the PCR products. PCR product curves were linear across serial 10-fold dilutions, and the melting curve analysis indicated the synthesis of a single homogeneous product with the expected melting temperature. The reactions were carried out with 20-μl capillaries containing 7.0 mM Mg^{2+}, a 10 pM concentration each of forward and reverse primers, 4.0 μl of LightCycler RT-PCR mix SYBR green I (LightCycler-RNA amplification kit SYBR green I; Roche), 2 μl of resolution solution, 0.4 μl of LightCycler RT-PCR enzyme mix, sterile H_2O, and 0.5 μg of total RNA. RT-PCR conditions for VP2 and GAPDH were as follows: reverse transcription at 55°C for 10 min, denaturation at 95°C for 2 min, and 40 cycles of amplification. Amplification conditions were as follows: denaturation to 95°C at 20°C/s without a plateau phase, annealing at 57°C for 7 s, and extension at 72°C for 15 s. The accumulation of products was monitored by SYBR green fluorescence at the completion of each cycle. There was a direct relationship between the cycle number at which the accumulation of PCR products became exponential and the log concentration of RNA molecules initially present in the RT-PCR. The reaction conditions for melting curve analysis were as follows: denaturation to 95°C at 20°C/s without a plateau phase, annealing at 60°C for 5 s, and denaturation to 95°C at 0.1°C/s, with continuous monitoring of SYBR green fluorescence. RNA samples ($n = 82$) from DAV-infected mice were analyzed for GAPDH mRNA levels to determine the levels of mRNA per sample and to confirm technical reproducibility. The GAPDH mRNA copy number per sample was 7.19 ± 0.02 $\log_{10}$ (mean and standard error of the mean). Therefore, the marked variations in virus RNA levels in individual samples could not be attributed to differences in amplifiable material. The amount of virus RNA was expressed as $\log_{10}$ viral VP2 copy number/0.5 μg of total RNA.

In vitro protection assays. NSC34 motor neurons, provided by Neil Cashman (University of Toronto, Toronto, Ontario, Canada), were grown in Dulbecco modified Eagle medium (DMEM) supplemented with 10% fecal calf serum and 1% Pen-Strep as previously described (42). Cells were allowed to differentiate in DMEM-F12 medium (50:50) supplemented with 1% fecal calf serum, 1% nonessential amino acids, and 1% Pen-Strep (5, 11). Following several passages under these conditions, the cells exhibited neurites and were considered to be differentiated to a motor neuron phenotype. Such differentiated cells were plated on 12-well plates, grown overnight to obtain greater than 80% confluence, and then infected with 1.5 PFU of TMEV per cell. At the time of infection, the cells were treated with IFN-γ (100 ng/ml) or left untreated. Following overnight incubation, cell survival was measured by using a standard MTT assay. Survival was calculated by normalizing the absorbance at 570 nm measured for treated cultures to the value obtained for uninfected, untreated cultures as previously described (42).

Likewise, spinal motor neuron cultures derived from neonatal B10.D1-H2^{q}/SgJ mice were prepared and cultured as previously described (42). Following 2 weeks of culturing, the cells were treated as described above, and cell survival following IFN-γ treatment was assessed by an MTT assay We used immunohistochemical analysis to detect virus antigen, and staining showed that all cells were infected with TMEV.

Viral mRNA levels were quantified with a LightCycler as previously described (42). Total RNA was isolated from NSC34 cell cultures treated as described above by using RNA-Stat60. Total RNA (0.15 μg) was amplified by using VP2-specific or GAPDH-specific primers as described above, and the generation of a specific product was measured and normalized. Absolute copy numbers were converted to $\log_{10}$ mRNA copy numbers for analysis.

Statistics. Data were analyzed by using either the Student t test for normally distributed data or the Mann-Whitney rank sum test for data that were not normally distributed. For comparisons of more than one group, analysis of variance was used. The Tukey test was used for all pairwise multiple-comparisons procedures. Proportional data were evaluated by using the z test. The level of significance was set at a P value of <0.05 for all tests.

RESULTS

IFN-$\gamma^{-/-}$ mice with normally resistant *H-2*^{b} MHC clear early virus infection in neurons but later develop virus persistence in the white matter and demyelination. Injection of TMEV into the CNS of mice results in two distinct disease phenotypes. Mice of the resistant *H-2*^{b}, *H-2*^{k}, and *H-2*^{d} haplotypes develop acute encephalitis at 7 to 10 days after infection, with virus replication restricted primarily to the hippocampus, striatum, and spinal cord neurons (50). The virus is then rapidly cleared such that persistence does not develop and demyelination does not ensue. In contrast, mice of the susceptible *H-2*^{s}, *H-2*^{v}, *H-2*^{q}, *H-2*^{u}, and *H-2*^{r} haplotypes develop similar acute encephalitis, but this condition is followed by incomplete clearance of the virus and subsequent chronic demyelinating disease in the spinal cord beginning 35 to 45 days after infection (45). The mechanism of resistance to virus persistence and demyelination is dependent upon the development of a rapid virus-specific class I-restricted cytotoxic lymphocyte response directed against viral capsid antigen (8, 23, 47). We tested whether genetic disruption of IFN-γ would convert normally resistant *H-2*^{b} mice to a susceptible phenotype.

TMEV-infected IFN-$\gamma^{-/-}$ *H-2*^{b} mice had no increased mortality compared to IFN-$\gamma^{+/+}$ *H-2*^{b} control mice (Fig. 1). The majority of mice survived the early infection. Analysis of the

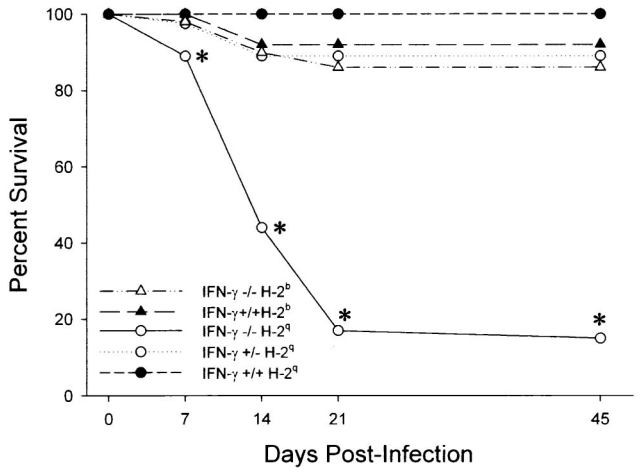

FIG. 1. IFN-γ decreases survival of *H-2*^{q} mice infected with TMEV. Survival of IFN-$\gamma^{-/-}$ *H-2*^{b} ($n = 101$), IFN-$\gamma^{+/+}$ *H-2*^{b} ($n = 65$), IFN-$\gamma^{-/-}$ *H-2*^{q} ($n = 51$), IFN-$\gamma^{+/-}$ *H-2*^{q} ($n = 40$), and IFN-$\gamma^{+/+}$ *H-2*^{q} ($n = 140$) mice infected intracranially with TMEV was analyzed. There was a statistically significant decrease in the survival of IFN-$\gamma^{-/-}$ mice of susceptible MHC haplotype *H-2*^{q} at 7, 14, 21, and 45 days compared to *H-2*^{q} mice with normal expression of IFN-γ ($P < 0.001$, as determined by the *z* test; asterisks). In contrast, mice of normally resistant MHC haplotype *H-2*^{b} showed no significant decrease in survival irrespective of IFN-γ expression.

spinal cord at 7 days after infection showed paradoxically more gray matter disease in IFN-$\gamma^{+/+}$ *H-2*^{b} mice than in IFN-$\gamma^{-/-}$ *H-2*^{b} mice ($P = 0.001$, as determined by the rank sum test) (Table 1). This pathologic finding most likely is explained by an increased presence of cytotoxic lymphocytes directed against viral antigen in the gray matter of IFN-$\gamma^{+/+}$ *H-2*^{b} mice (23). Of interest, by 16 days after infection, there was no evidence of gray matter disease in the spinal cords of either IFN-$\gamma^{-/-}$ *H-2*^{b} or IFN-$\gamma^{+/+}$ *H-2*^{b} mice (Table 1 and Fig. 2A). Only minimal or no demyelination was observed in IFN-$\gamma^{+/+}$ *H-2*^{b} control mice at 7, 16, 21, or 45 days after infection (Table 1 and Fig. 2B). IFN-$\gamma^{-/-}$ *H-2*^{b} mice showed no or minimal evidence of spinal cord gray matter pathologic changes at 7 days after infection

TABLE 1. Spinal cord pathologic changes in IFN-$\gamma^{-/-}$ mice of *H-2*^{b} haplotype

Day	Mice (no. tested)	Mean ± SEM score for:		
		Inflammation		Demyelination
		Gray matter	White matter	
7	IFN-$\gamma^{-/-}$ (9)	3.6 ± 1.1[a]	1.3 ± 0.5	0.0 ± 0.0
	IFN-$\gamma^{+/+}$ (7)	19.1 ± 4.8	2.1 ± 0.8	0.0 ± 0.0
16	IFN-$\gamma^{-/-}$ (9)	0.0 ± 0.0	0.0 ± 0.0	0.0 ± 0.0
	IFN-$\gamma^{+/+}$ (7)	0.0 ± 0.0	1.1 ± 0.6	0.0 ± 0.0
21	IFN-$\gamma^{-/-}$ (16)	0.0 ± 0.0	1.3 ± 0.6	2.5 ± 0.9
	IFN-$\gamma^{+/+}$ (10)	0.2 ± 0.2	0.0 ± 0.0	0.2 ± 0.2
45	IFN-$\gamma^{-/-}$ (8)	1.2 ± 0.7	5.1 ± 2.1	13.9 ± 4.7
	IFN-$\gamma^{+/+}$ (8)	0.0 ± 0.0	0.0 ± 0.0	0.0 ± 0.0

[a] Significantly different from values for IFN-$\gamma^{+/+}$ mice at 7 days postinfection, as determined by Mann-Whitney rank sum test ($P = 0.001$).

(Fig. 2C). In contrast, IFN-$\gamma^{-/-}$ *H-2*^{b} mice developed demyelination in the spinal cord beginning at 21 days (demyelination score, 2.5 ± 0.9 [mean and standard error of the mean]) and progressing in severity to 45 days (demyelination score, 13.9 ± 4.7) after infection (Table 1 and Fig. 2D). By 45 days after infection, six of eight IFN-$\gamma^{-/-}$ *H-2*^{b} mice showed demyelination in the spinal cord (Fig. 2D). In contrast, none of eight IFN-$\gamma^{+/+}$ *H-2*^{b} mice showed demyelination at this time (Fig. 2B). We conclude that genetic deletion of IFN-γ in *H-2*^{b} mice had no effect on the clearance of early gray matter disease in neurons but did result in the inhibition of resistance to white matter disease, since mice developed chronic virus persistence in glial cells and inflammatory demyelination.

IFN-γ disruption in susceptible *H-2*^{q} mice results in marked clinical deficits and early death following TMEV infection. To address the function of IFN-γ in animals of the susceptible haplotype, we crossed IFN-$\gamma^{-/-}$ *H-2*^{b} mice to IFN-$\gamma^{+/+}$ *H-2*^{q} B10.D1-H2^q/SgJ mice. An F_2 generation was produced, and animals homozygous for IFN-$\gamma^{-/-}$ and *H-2*^{q} were selected. These mice were intercrossed to generate a line of IFN-$\gamma^{-/-}$ *H-2*^{q} mice and a line of IFN-$\gamma^{+/+}$ *H-2*^{q} mice. Following TMEV infection, IFN-$\gamma^{-/-}$ *H-2*^{q} mice showed a dramatic decrease in survival compared to IFN-$\gamma^{+/+}$ *H-2*^{q} mice and IFN-$\gamma^{+/-}$ *H-2*^{q} mice. Of 32 IFN-$\gamma^{-/-}$ *H-2*^{q} mice, 18 died by 2 weeks postinfection (Fig. 1). Most deaths occurred during the first 12 days after infection. This finding implied that animals likely were dying as a result of the early neuronal disease seen with this model. In contrast, no deaths were reported for 130 IFN-$\gamma^{+/+}$ *H-2*^{q} mice, and only 4 of 36 IFN-$\gamma^{+/-}$ *H-2*^{q} mice were dead by 2 weeks. IFN-$\gamma^{-/-}$ *H-2*^{q} animals also showed major clinical deficits characterized by incoordination, motor hind limb weakness or paralysis, scruffy fur, and poor general appearance. Thirteen percent of the mice survived until day 45, a time traditionally used in this model to determine the presence or absence of chronic demyelinating disease (47). Mice that survived the acute neuronal disease exhibited severe neurologic deficits.

IFN-$\gamma^{-/-}$ *H-2*^{q} mice develop a normal humoral immune response directed against TMEV. IFN-γ has been shown to play an important role in influencing the function of class II-restricted helper T cells in enhancing antibody production and participating in isotype switching (15, 54). Therefore, a deficiency in this cytokine from birth theoretically could affect the protective humoral response directed against TMEV and could lead to reduced survival and enhancement of clinical deficits. To test these possibilities, we assessed antibody responses in serum by using an ELISA directed against purified virus antigens (Fig. 3). Serum IgM (Fig. 3A) and IgG (Fig. 3B) responses were measured at 14 to 18 days after infection. Similar IgM responses were observed in IFN-$\gamma^{-/-}$ *H-2*^{q}, IFN-$\gamma^{+/-}$ *H-2*^{q}, and IFN-$\gamma^{+/+}$ *H-2*^{q} mice. All strains of mice developed similar IgG responses to purified virus. In contrast, noninfected littermate controls showed no antiviral antibody responses. To address this issue further, we analyzed virus-specific neutralization at this time by using antiserum from IFN-$\gamma^{+/+}$ *H-2*^{q}, IFN-$\gamma^{+/-}$ *H-2*^{q}, and IFN-$\gamma^{-/-}$ *H-2*^{q} mice. The neutralization titers (expressed as $\log_2$ units) were 7.00 ± 0.63 ($n = 5$; mean and standard error of the mean) for IFN-$\gamma^{-/-}$ *H-2*^{q}, 7.63 ± 0.55 ($n = 4$) for IFN-$\gamma^{+/-}$ *H-2*^{q}, and 8.8 ± 0.2 ($n = 5$) for IFN-$\gamma^{+/+}$ *H-2*^{q} mice. Even though there was a ten-

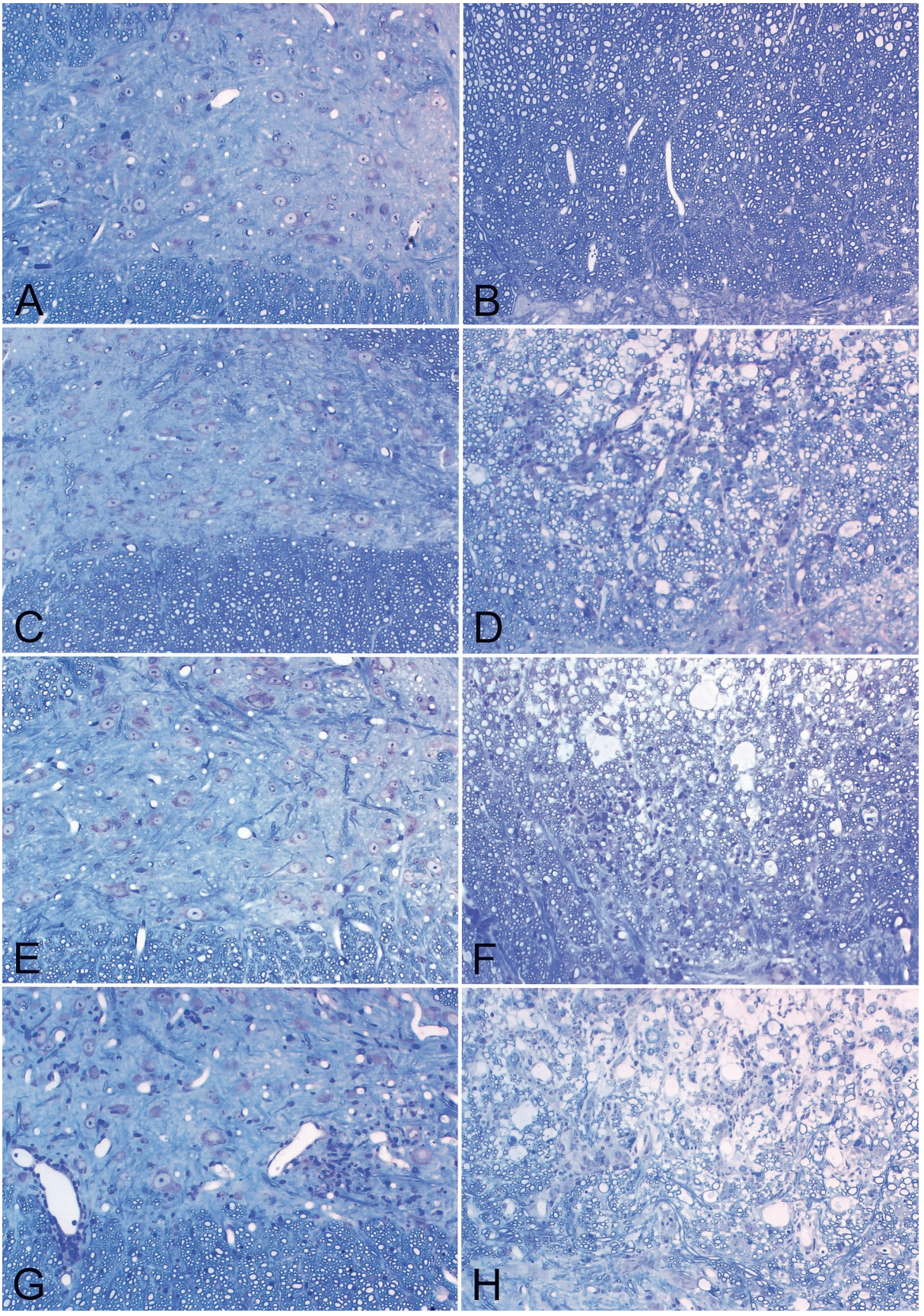
A
B
C
D
E
F
G
H

dency for IFN-$\gamma^{+/+}$ *H-2*^{q} mice to have higher neutralization titers, this finding was not statistically significant. We conclude from these experiments that a deficit in IFN-γ did not affect the normal humoral response to TMEV and was not the explanation for the increased mortality observed in IFN-$\gamma^{-/-}$ *H-2*^{q} mice.

IFN-γ-deficient mice show reduced expression of CD4, CD8, class I MHC, and class II MHC antigens in the spinal cord gray matter following infection with TMEV. IFN-γ has major effects on the immune system, including the up-regulation of class II MHC antigens on microglia, the promotion of leukocyte adhesion, induction of the expression of costimulatory molecules, and an influence on "helper" T-cell development (34). Therefore, deletion of IFN-γ from birth might have altered the immune responses to virus antigens outside and inside the nervous system. Further, we wondered whether an IFN-γ deficiency in *H-2*^{q} mice altered the distribution of T cells or the expression of MHC in the CNS following virus infection (Fig. 4). Immunostaining was performed on spinal cord sections from IFN-$\gamma^{-/-}$ and IFN-$\gamma^{+/-}$ mice. CD4 (Fig. 4A and C) and CD8 (Fig. 4B and D) T cells were observed in the spinal cords of both strains of mice. As described previously (27), CD4 cells were found mostly in a perivascular location (Fig. 4A and C), whereas CD8 cells (Fig. 4B and D) were scattered away from blood vessels throughout the parenchyma. In general, at 16 days after infection, there was a dramatic reduction in CD4 and CD8 expression in the spinal cord gray matter of IFN-$\gamma^{-/-}$ *H-2*^{q} mice (Fig. 4B and D) compared to IFN-$\gamma^{+/+}$ *H-2*^{q} mice (Fig. 4A and C). However, the distribution of F4/80, which marks microglia and a subset of macrophages, was not different between IFN-$\gamma^{-/-}$ *H-2*^{q} mice and IFN-$\gamma^{+/+}$ *H-2*^{q} mice (Fig. 4I and J). Class I MHC immunostaining was distributed within the lesion in blood vessels and in cells with presumed glial morphology (Fig. 4E and F). Class II MHC immunostaining (Fig. 4G and H) was expressed in cells with a morphology consistent with macrophages and microglia. Deletion of IFN-γ resulted in decreased expression of both class I MHC and class II MHC in IFN-$\gamma^{-/-}$ *H-2*^{q} mice (Fig. 4F and H) compared to IFN-$\gamma^{+/+}$ *H-2*^{q} mice (Fig. 4E and H). The results support the hypothesis that one reason for decreased survival and neuronal spinal cord disease in IFN-$\gamma^{-/-}$ *H-2*^{q} mice compared to IFN-$\gamma^{+/+}$ *H-2*^{q} mice is an impaired cellular immune response to the virus.

IFN-$\gamma^{-/-}$ *H-2*^{q} mice show severe pathologic changes in the spinal cord gray matter at 11 to 17 days after infection. Given the different adaptive cellular immune responses in the animals tested, we undertook a detailed morphologic analysis of IFN-$\gamma^{-/-}$ *H-2*^{q} mice, IFN-$\gamma^{+/-}$ *H-2*^{q} mice, and parental IFN-$\gamma^{+/+}$ *H-2*^{q} mice at 7, 11 to 17, and 21 days after infection. We investigated the reason for the high mortality in infected IFN-$\gamma^{-/-}$ *H-2*^{q} mice (Table 2 and Fig. 1). Between 11 and 17 days after infection, many IFN-$\gamma^{-/-}$ *H-2*^{q} mice were clinically ill or moribund. For this reason, the animals were sacrificed during this time period in accordance with Mayo Clinic Animal Care Institutional Policy. There was no difference at 7 days postin-

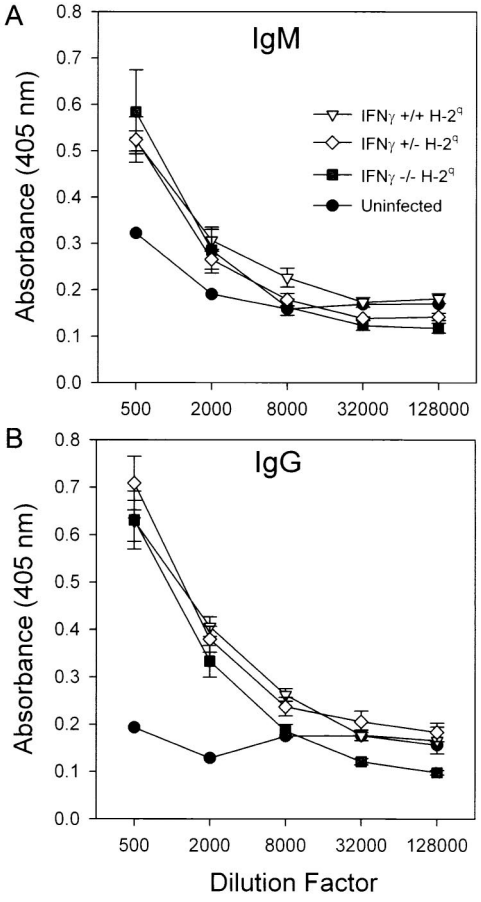

FIG. 3. IFN-γ does not affect the TMEV-specific IgM or IgM response in TMEV-infected *H-2*^{q} mice. (A) ELISA for serum IgM antibodies (11 to 16 days after infection) directed against purified TMEV antigens in IFN-$\gamma^{-/-}$ *H-2*^{q}, IFN-$\gamma^{+/+}$ *H-2*^{q}, and IFN-$\gamma^{+/-}$ *H-2*^{q} mice. Negative controls were from mice not infected with TMEV. IFN-$\gamma^{-/-}$, IFN-$\gamma^{+/-}$, and IFN-$\gamma^{+/+}$ mice developed normal humoral antibody responses to the virus antigens. IFN-$\gamma^{-/-}$ *H-2*^{q} mice had IgM responses at 11 to 16 days similar to those of the other experimental groups, even though these mice had profound neurologic deficits and frequent deaths at these times after infection. (B) Virus-specific IgG ELISA at 11 to 16 days postinfection. This assay also showed no differences between groups. Error bars indicate standard error of the mean.

FIG. 2. IFN-γ deficiency inhibits resistance to spinal cord demyelination in *H-2*^{b} mice and increases gray matter disease in *H-2*^{q} mice infected with TMEV. Spinal cord pathologic changes following TMEV infection were evaluated (glycol methacrylate plastic-embedded sections stained with modified Erichrome-cresyl violet stain). (A) Absence of neuronal disease during early infection in an IFN-$\gamma^{+/+}$ *H-2*^{b} mouse (7 days). (B) Absence of demyelination in an IFN-$\gamma^{+/+}$ *H-2*^{b} mouse (45 days). (C) Absence of neuronal disease in an IFN-$\gamma^{-/-}$ *H-2*^{b} mouse (7 days). (D) Presence of white matter inflammation and demyelination in an IFN-$\gamma^{-/-}$ *H-2*^{b} mouse (45 days) (E) Absence of neuronal disease in an IFN-$\gamma^{+/+}$ *H-2*^{q} mouse (7 days). (F) Presence of white matter inflammation and demyelination in an IFN-$\gamma^{+/+}$ *H-2*^{q} mouse (45 days). (G) Presence of gray matter neuronal disease with inflammatory infiltrates in an IFN-$\gamma^{-/-}$ *H-2*^{q} mouse (7 days). Note the loss of anterior horn cells compared to what is shown in spinal cord sections in panels A, C, and E. (H) Presence of white matter inflammation and demyelination in an IFN-$\gamma^{-/-}$ *H-2*^{q} mouse (45 days).

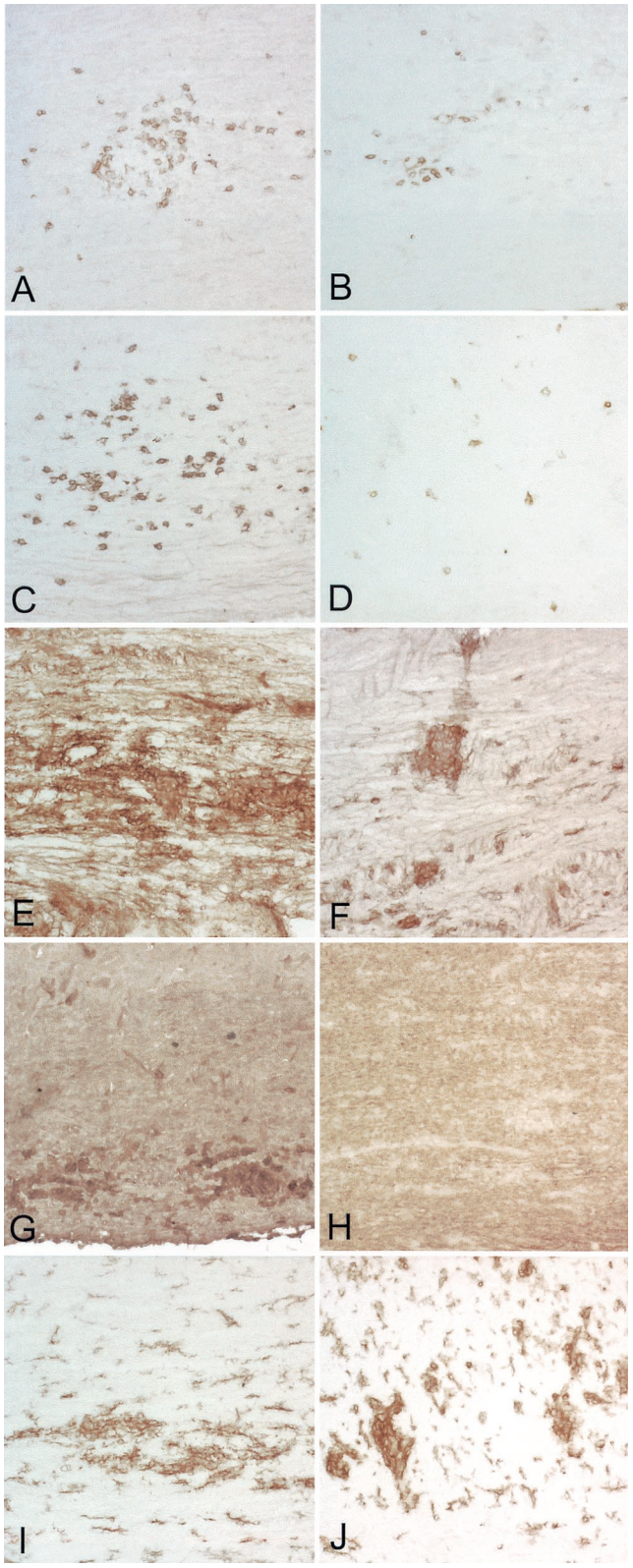

FIG. 4. Decreased CD4, CD8, class I MHC, and class II MHC expression in spinal cords of IFN$^{-/-}$ *H-2*^{q} mice. Immunoperoxidase staining for CD4^{+} T cells, CD8^{+} T cells, class I MHC, class II MHC, and F4/80 (macrophages) in spinal cords of IFN$^{-/-}$ *H-2*^{q} and IFN$^{+/+}$ *H-2*^{q} mice was carried out at 12 days after infection. (A) CD4^{+} T cells are abundant in the spinal cord of an IFN-$\gamma^{+/+}$ *H-2*^{q} mouse. Some of the CD4^{+} T cells are present in the meninges, whereas others are present in the parenchyma, frequently in a perivascular location. (B) There are fewer CD4^{+} T cells in the spinal cord of an IFN-$\gamma^{-/-}$ *H-2*^{q} mouse than in comparable areas of the spinal cord of an IFN-$\gamma^{+/+}$ mouse (panel A). (C) A serial section from an IFN-$\gamma^{+/+}$ *H-2*^{q} mouse (panel A) was stained for CD8^{+} T cells. Note that the cells are distributed widely in the spinal cord parenchyma and have a distinct distribution compared to CD4^{+} T cells. (D) A serial section from an IFN-$\gamma^{-/-}$ *H-2*^{q} mouse (panel B) shows that there are fewer CD8^{+} T cells than in an IFN-$\gamma^{+/+}$ *H-2*^{q} mouse (panel C). (E) Class I MHC-positive cells are present almost exclusively in the gray matter of the spinal cord of an IFN-$\gamma^{+/+}$ *H-2*^{q} mouse. (F) There is less expression of class I MHC in cells of the gray matter of an IFN-$\gamma^{-/-}$ than in an IFN-$\gamma^{+/+}$ *H-2*^{q} mouse (panel E). (G) A serial section (obtained from the sample shown in panel E) shows the localization of class II MHC-positive cells in an IFN-$\gamma^{+/+}$ *H-2*^{q} mouse. The cells are widely scattered in the gray matter and in the white matter. (H) A serial section (obtained from the sample shown in panel F) shows less expression of class II MHC-positive cells in the spinal cord of an IFN-$\gamma^{-/-}$ mouse than in that of an IFN-$\gamma^{+/+}$ mouse. (I) Staining in an IFN-$\gamma^{+/+}$ *H-2*^{q} mouse for F4/80 demonstrates labeling of macrophages and a subpopulation of microglia. (J) An extent of F4/80 staining similar to that shown in panel I was observed in an IFN-$\gamma^{+/-}$ mouse.

TABLE 2. Spinal cord pathologic changes in IFN-$\gamma^{-/-}$ mice of *H-2*^{q} haplotype

Day	Mice (no. tested)	Mean ± SEM score for:		
		Inflammation		Demyelination
		Gray matter	White matter	
7	IFN-$\gamma^{-/-}$ (5)	7.8 ± 3.7	3.1 ± 2.1	0.0 ± 0.0
	IFN-$\gamma^{+/-}$ (6)	6.4 ± 3.6	4.0 ± 2.0	0.0 ± 0.0
	IFN-$\gamma^{+/+}$ (2)	8.6 ± 8.6	7.2 ± 4.9	0.0 ± 0.0
11–17	IFN-$\gamma^{-/-}$ (16)	24.7 ± 4.6[a]	3.8 ± 1.8	0.0 ± 0.0
	IFN-$\gamma^{+/-}$ (7)	5.7 ± 1.3	1.6 ± 0.8	0.0 ± 0.0
16	IFN-$\gamma^{+/+}$ (7)	0.5 ± 0.3	2.4 ± 1.0	2.0 ± 0.6
21	IFN-$\gamma^{-/-}$ (10)	6.1 ± 3.4	5.6 ± 1.5	4.1 ± 1.5
	IFN-$\gamma^{+/-}$ (7)	5.4 ± 4.3	4.9 ± 3.0	4.1 ± 2.4
	IFN-$\gamma^{+/+}$ (14)	0.0 ± 0.0	3.0 ± 1.3	2.6 ± 1.6

[a] Significantly different from values for IFN-$\gamma^{+/-}$ and IFN-$\gamma^{+/+}$ mice, as determined by Mann-Whitney rank sum test ($P = 0.016$ and $P = 0.005$, respectively).

fection in the extent of gray matter pathologic changes for IFN-$\gamma^{+/+}$, IFN-$\gamma^{+/-}$, and IFN-$\gamma^{+/+}$ *H-2*^{q} mice (Table 2). However, at 11 to 17 days postinfection, we found four- to fivefold increases in the percentages of spinal cord quadrants with gray matter disease for IFN-$\gamma^{-/-}$ *H-2*^{q} mice (24.7% ± 4.6% [mean and standard error of the mean]) compared to IFN-$\gamma^{+/-}$ *H-2*^{q} mice (5.7% ± 1.3%) ($P < 0.016$, as determined by the rank sum test). An even greater difference was observed when IFN-$\gamma^{-/-}$ *H-2*^{q} mice were compared to parental IFN-$\gamma^{+/+}$ *H-2*^{q} mice (0.5% ± 1.3%) ($P = 0.005$, as determined by the rank sum test). Multiple examples of anterior horn neurons undergoing cell death were observed in IFN-$\gamma^{-/-}$ *H-2*^{q} mice (Fig. 5B). Neuronophagia, as demonstrated by macrophages and other inflammatory cells engulfing neuronal debris, was observed in IFN-$\gamma^{-/-}$ *H-2*^{q} mice (Fig. 5B) but not in IFN-$\gamma^{+/-}$ *H-2*^{q} mice (Fig. 5A) or parental IFN-$\gamma^{+/+}$ *H-2*^{q} mice. At 11 to 17 days after infection, there was no significant difference in

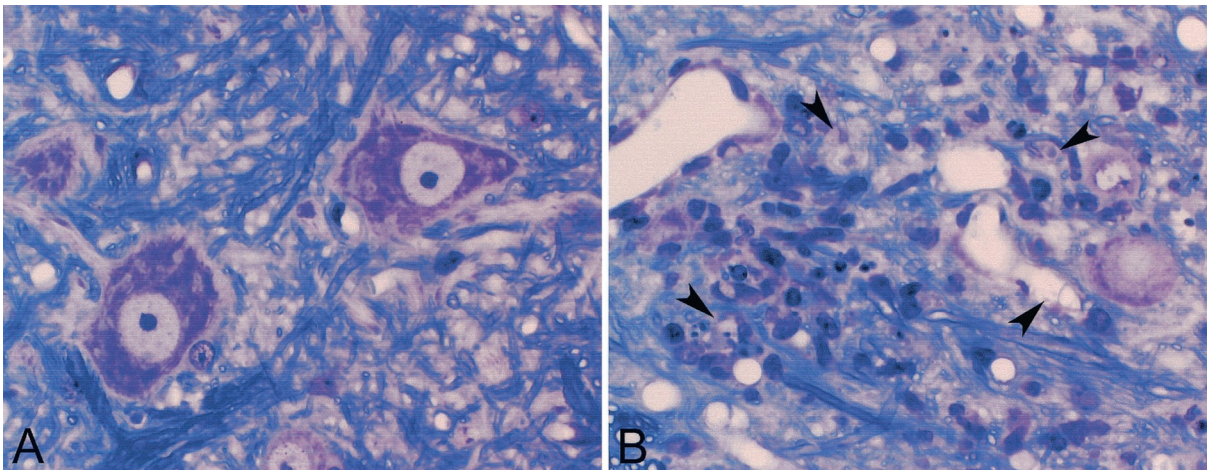

FIG. 5. IFN-γ in *H-2*^{q} mice protects spinal neurons from death. (A) Normal anterior horn cell neurons in an IFN-γ$^{+/-}$ *H-2*^{q} mouse at 21 days after TMEV infection. (B) Anterior horn cell loss in an IFN-γ$^{-/-}$ *H-2*^{q} mouse at 13 days after TMEV infection. Arrowheads indicate remnants of anterior horn cells along with intense inflammatory infiltration. No examples of anterior horn cell death like that shown here were observed in IFN-γ$^{+/+}$ *H-2*^{q} or IFN-γ$^{+/-}$ *H-2*^{q} mice following TMEV infection.

the percentages of spinal cord quadrants showing white matter inflammation or demyelination in the various mouse strains. We also studied 10 IFN-γ$^{-/-}$ *H-2*^{q} mice that survived to 21 days postinfection. At this time, there was no difference in the extent of gray matter pathologic changes in IFN-γ$^{-/-}$ *H-2*^{q} and IFN-γ$^{+/-}$ *H-2*^{q} mice (Table 2). This finding was likely the result of selective analysis of IFN-γ$^{-/-}$ *H-2*^{q} mice that survived the severe neuronal infection. However, both IFN-γ$^{-/-}$ *H-2*^{q} mice and IFN-γ$^{+/-}$ *H-2*^{q} mice showed some degree of gray matter disease, but this degree of disease was not statistically significant compared to the findings for IFN-γ$^{+/+}$ *H-2*^{q} mice, which showed no gray matter pathologic changes at 21 days (Table 2). By 21 days, early demyelination was beginning to occur in the white matter of the spinal cord in all strains. There was a tendency for both IFN-γ$^{-/-}$ *H-2*^{q} mice and IFN-γ$^{+/-}$ *H-2*^{q} mice to show more quadrants with demyelination than parental IFN-γ$^{+/+}$ *H-2*^{q} mice, but this tendency was not statistically significant (Table 2). Both IFN-γ$^{+/+}$ *H-2*^{q} mice (Fig. 2F) and IFN-γ$^{-/-}$ *H-2*^{q} mice (Fig. 2H) showed extensive demyelination at 45 days after infection. Thus, the experiment indicated that one of the primary reasons that IFN-γ$^{-/-}$ *H-2*^{q} mice developed marked neurologic deficits and early deaths likely was injury of anterior horn cells in the gray matter of the spinal cord during the first 2 weeks of infection.

TMEV-infected IFN-γ$^{-/-}$ *H-2*^{q} mice do not show more severe disease in the brain. Having established that IFN-γ deficiency predisposed *H-2*^{q} mice to spinal cord gray matter neuronal injury, we wondered whether IFN-γ deficiency would predispose specific populations of brain neurons to virus-induced injury. We analyzed the brains of IFN-γ$^{+/+}$ *H-2*^{q} mice, IFN-γ$^{+/-}$ *H-2*^{q} mice, and IFN-γ$^{-/-}$ *H-2*^{q} mice for the severity of pathologic injuries to areas of the brain. Analysis was done at 7 days to establish whether brain disease was established in the various mouse strains to a similar extent. We also analyzed the brain at 16 days after infection, a time when IFN-γ$^{-/-}$ *H-2*^{q} mice were dying but IFN-γ$^{+/-}$ *H-2*^{q} and IFN-γ$^{+/+}$ *H-2*^{q} mice were not. We used a semiquantitative 4-point scale for analysis. All three strains of mice showed pathologic changes in the cortex, hippocampus, striatum, and corpus callosum at 7 and 16 days after infection, whereas there was no or minimal disease in the cerebellum. However, there were no differences in the distribution or severity of brain disease in the various mouse strains at either 7 days or 16 days after TMEV infection (data not shown). Therefore, the reason for prominent neurologic deficits and early deaths in IFN-γ$^{-/-}$ *H-2*^{q} mice compared to IFN-γ$^{+/-}$ *H-2*^{q} and IFN-γ$^{+/+}$ *H-2*^{q} mice was not more severe brain disease. Thus, the protective effect of IFN-γ was specific to anterior horn cells in the spinal cord.

IFN-γ$^{-/-}$ *H-2*^{q} mice propagate more virus RNA in the spinal cord. Recent reports indicated that virus RNA persists following TMEV infection during chronic disease even though it is often difficult to detect infectious virus by plaque assays (55). We developed a sensitive and quantitative RT-PCR assay that allowed us to measure the copy numbers of VP2 RNA in the brains and spinal cords of infected IFN-γ-deficient mice (Fig. 6). We evaluated the levels of virus RNA expression in the brains and spinal cords independently. All experiments were controlled by measuring GAPDH mRNA expression levels, which were highly consistent among strains and times after virus infection. In the 82 mice examined, the GAPDH RNA copy number was 7.19 ± 0.02 $\log_{10}$ (mean and standard error of the mean). At 7 days after infection, the VP2 copy number in the brains and spinal cords of IFN-γ$^{-/-}$ *H-2*^{q} mice and parental IFN-γ$^{+/+}$ *H-2*^{q} mice was approximately 7 $\log_{10}$. At 7 days, there was a statistically significant difference ($P = 0.0.27$) in virus RNA copy number between IFN-γ$^{-/-}$ *H-2*^{q} mice and IFN-γ$^{+/+}$ *H-2*^{q} mice. By 14 days after infection, the virus RNA copy numbers in the brains (5.76 ± 0.11 $\log_{10}$) and spinal cords (6.17 ± 0.04 $\log_{10}$) of IFN-γ$^{+/+}$ *H-2*^{q} mice had decreased by approximately 100-fold compared to those at 7 days (brain, 6.94 ± 0.09 $\log_{10}$; spinal cord, 7.01 ± 0.11 $\log_{10}$). In contrast, by 14 days in IFN-γ$^{-/-}$ *H-2*^{q} mice, the virus RNA copy numbers had not decreased in the brains (7.04 ± 0.19 $\log_{10}$) and spinal cords (7.13 ± 0.11 $\log_{10}$) compared to those at 7 days (brain, 7.45 ± 0.08 $\log_{10}$; spinal cord, 6.97 ± 0.12 $\log_{10}$), consistent with the failure of clearance of virus. At 14 days after

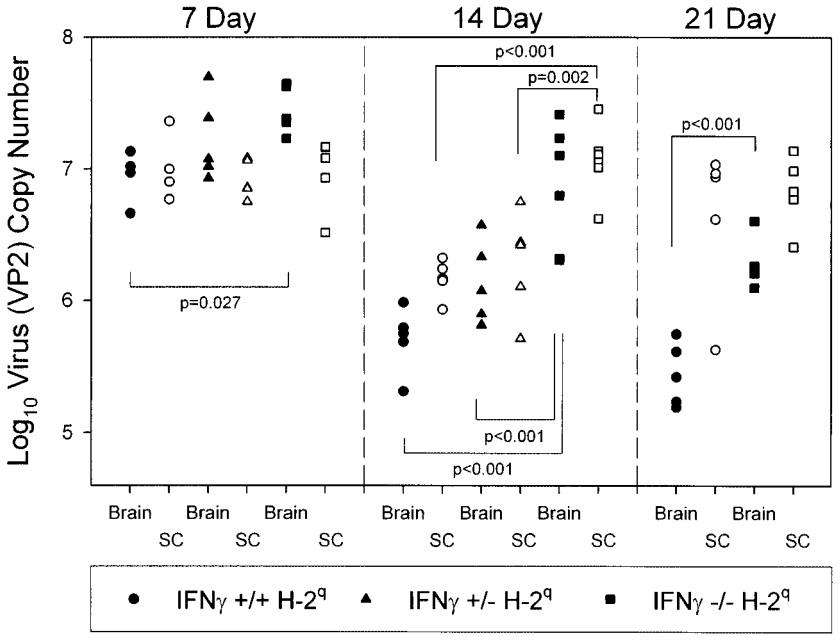

FIG. 6. IFN-γ decreases virus RNA levels in the CNS of TMEV-infected *H-2*^{q} mice. Levels of virus RNA expression at 7, 14, and 21 days after TMEV infection in the brains and spinal cords (SC) of IFN-$\gamma^{+/+}$ *H-2*^{q} mice, IFN-$\gamma^{+/-}$ *H-2*^{q} mice, and IFN-$\gamma^{-/-}$ *H-2*^{q} mice were analyzed independently. Levels of viral capsid VP2 RNA were quantified with LightCycler PCR. Statistical differences, determined with the Student *t* test, between the groups are shown with respective *P* values. Each symbol on the graph represents an individual animal. The levels of expression of GAPDH RNA were consistent among the groups (mean $\log_{10}$ units, 7.19 ± 0.02).

infection, the difference in virus RNA copy number between IFN-$\gamma^{-/-}$ *H-2*^{q} mice and IFN-$\gamma^{+/+}$ *H-2*^{q} mice was highly statistically significant ($P < 0.001$ for brain and $P < 0.001$ for spinal cord). In addition, there was a highly statistically significant difference for virus RNA copy number between IFN-$\gamma^{-/-}$ *H-2*^{q} mice and IFN-$\gamma^{+/-}$ *H-2*^{q} mice ($P = 0.002$ for brain and $P < 0.001$ for spinal cord). By 21 days after infection, the virus RNA copy number in the brains of IFN-$\gamma^{-/-}$ *H-2*^{q} mice (6.32 ± 0.09 $\log_{10}$) was higher than that in the brains of IFN-$\gamma^{+/+}$ *H-2*^{q} mice (5.45 ± 0.04 $\log_{10}$) ($P < 0.001$). However, both IFN-$\gamma^{-/-}$ *H-2*^{q} mice (6.64 ± 0.04 $\log_{10}$) and IFN-$\gamma^{+/+}$ *H-2*^{q} mice (6.89 ± 0.12 $\log_{10}$) had comparable levels of virus RNA in their spinal cords. The comparable levels of virus RNA in the spinal cords at this time are consistent with the observation that the expression of IFN-γ had no effect on the development of chronic spinal cord demyelination in mice of the susceptible *H-2*^{q} haplotype. The results support the hypothesis that in *H-2*^{q} mice, IFN-γ is critical for the clearance of a TMEV-specific message, particularly during the early course of infection.

IFN-γ deficiency in *H-2*^{q} mice permits prominent virus infection of anterior horn motor neurons in the spinal cord. We first examined the distribution of virus antigen in the spinal cords of IFN-$\gamma^{-/-}$ *H-2*^{b} and IFN-$\gamma^{+/+}$ *H-2*^{b} mice at 16 days after infection (Fig. 7A and B). For this analysis, we scored every spinal quadrant for the presence or absence of virus antigen-positive cells in either the gray matter or the white matter in every animal. No virus antigen-positive cells were observed in the spinal cord gray matter or white matter of normally resistant IFN-$\gamma^{+/+}$ *H-2*^{b} mice (Fig. 7A). No virus antigen-positive cells were observed in the spinal cord gray matter of nine IFN-$\gamma^{-/-}$ *H-2*^{b} mice (Fig. 7B). However, two of nine IFN-$\gamma^{-/-}$ *H-2*^{b} mice (Fig. 7B) did show a small number of virus antigen-positive cells in the white matter, consistent with the development of demyelination in these mice. We next examined the distribution of virus antigen in the spinal cords of IFN-$\gamma^{-/-}$ *H-2*^{q}, IFN-$\gamma^{+/-}$ *H-2*^{q}, and IFN-$\gamma^{+/+}$ *H-2*^{q} mice at 11 to 16 days after infection (Fig. 7C, D, and E). The percentage of gray matter quadrants demonstrating infected cells was higher in IFN-$\gamma^{-/-}$ *H-2*^{q} mice (30.2% ± 6.0% [mean and standard error of the mean]) (Fig. 7E) than in IFN-$\gamma^{+/-}$ *H-2*^{q} mice (9.4% ± 3.9%) (Fig. 7D) or IFN-$\gamma^{+/+}$ *H-2*^{q} mice (3.1% ± 1.3%) (Fig. 7C). These differences were statistically significant, as determined by a one-way analysis of variance ($P < 0.001$). Multiple comparisons with the Tukey test showed significant differences in the percentages of gray matter quadrants with virus-positive cells between IFN-$\gamma^{-/-}$ *H-2*^{q} mice and IFN-$\gamma^{+/-}$ *H-2*^{q} mice ($P = 0.009$) and between IFN-$\gamma^{-/-}$ *H-2*^{q} mice and IFN-$\gamma^{+/+}$ *H-2*^{q} mice ($P = 0.001$). At 11 to 16 days after infection, there was no significant difference in the percentages of spinal cord white matter quadrants showing virus antigen-positive cells in IFN-$\gamma^{-/-}$ *H-2*^{q} mice (24.7% ± 4.4%), IFN-$\gamma^{-/-}$ *H-2*^{q} mice (19.1% ± 5.6%), and IFN-$\gamma^{+/+}$ *H-2*^{q} mice (30.5% ± 5.7%). There was no statistically significant difference in the percentages of spinal cord gray matter versus white matter quadrants showing virus antigen-positive cells in IFN-$\gamma^{-/-}$ *H-2*^{q} mice and IFN-$\gamma^{+/-}$ *H-2*^{q} mice. However, there were 10-fold more quadrants with virus antigen-positive cells in the white matter of IFN-$\gamma^{+/+}$ *H-2*^{q} B10.D1-H2^q/SgJ mice than in the gray matter ($P < 0.001$, as determined by the Student *t* test).

The most unique finding was the localization of virus within the anterior horn cells of the spinal cord in IFN-$\gamma^{-/-}$ *H-2*^{q}

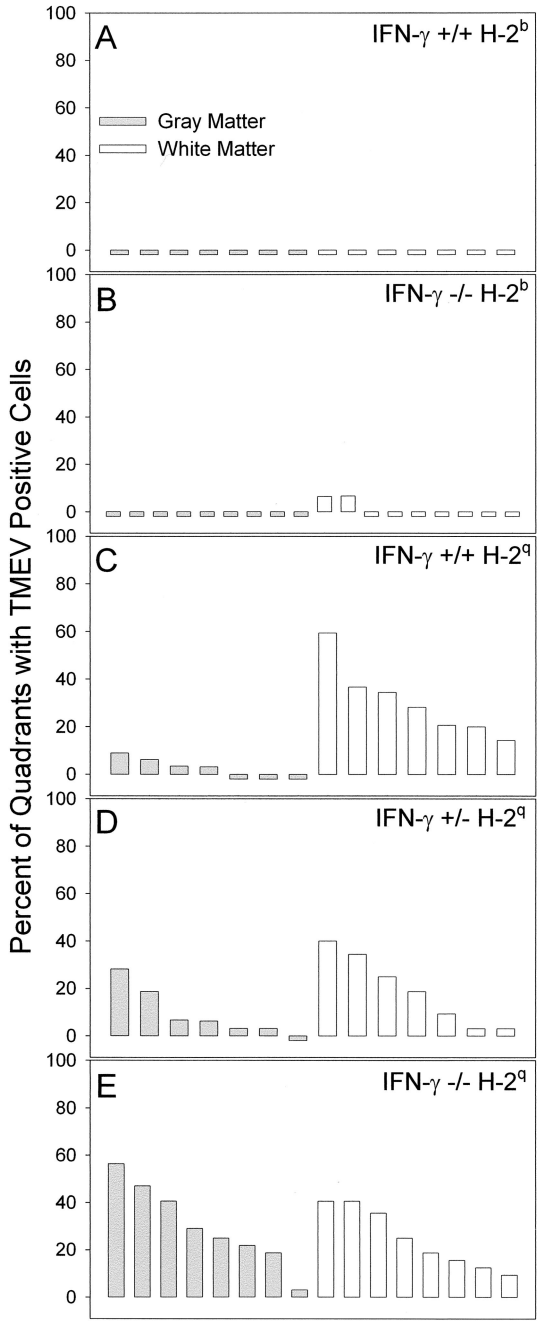

FIG. 7. Quantitation of spinal cord quadrants with TMEV-infected cells in the gray matter and white matter of the spinal cord. The number of virus antigen-positive cells was determined by immunoperoxidase staining and expressed as the percentage of spinal quadrants showing virus antigen-positive cells in either the gray matter or the white matter. Analysis was done 16 days after infection. Each bar represents one animal. (A) No virus-antigen positive cells were observed in the gray matter or the white matter of normally resistant IFN-$\gamma^{+/+}$ *H-2*^{b} mice. (B) In contrast, there were small numbers of virus antigen-positive cells in the white matter of two of nine IFN-$\gamma^{-/-}$ *H-2*^{b} mice but no virus antigen-positive cells in the gray matter. (C) A few virus antigen-positive cells were observed in four of seven IFN-$\gamma^{+/+}$ *H-2*^{q} mice, whereas multiple spinal cord quadrants showed virus antigen-positive cells in all seven of seven IFN-$\gamma^{+/+}$ *H-2*^{q} mice. (D) Similar distributions of virus antigen-positive cells were observed in IFN-$\gamma^{+/-}$*H-2*^{q} mice and IFN-$\gamma^{+/+}$ *H-2*^{q} mice. (E) In contrast, there were more spinal cord quadrants with virus antigen-positive cells in the gray matter of IFN-$\gamma^{-/-}$ *H-2*^{q} mice than in those of IFN-$\gamma^{+/+}$ *H-2*^{q} mice ($P = 0.001$, as determined by the Student *t* test) or in those of IFN-$\gamma^{+/-}$ *H-2*^{q} mice ($P = 0.015$, as determined by the Student *t* test).

mice at 11 to 16 days after infection (Fig. 8). In IFN-$\gamma^{+/+}$ *H-2*^{b} mice (Fig. 8A) and IFN-$\gamma^{-/-}$ *H-2*^{b} mice (Fig. 8C), there were no examples of virus antigen in spinal cord anterior horn cells. This finding indicated that in the resistant *H-2*^{b} haplotype, the expression of IFN-γ had no effect on the normal clearance of virus from anterior horn cells. We did see examples of presumed glial cells and macrophages expressing virus antigen in the white matter of IFN-$\gamma^{-/-}$ *H-2*^{b} mice (Fig. 8D) but not IFN-$\gamma^{+/+}$ *H-2*^{b} mice (Fig. 8B). In contrast, virus antigen in IFN-$\gamma^{-/-}$ *H-2*^{q} mice (Fig. 8G) was localized exclusively to the cytoplasm and major dendrites of anterior horn cells. For many of these cells, the morphology was sufficiently intact to identify the nucleoli. No examples of anterior horn motor neurons expressing virus antigen were identified in the IFN-$\gamma^{+/-}$ *H-2*^{q} mice or the IFN-$\gamma^{+/+}$ *H-2*^{q} mice (Fig. 8E). In the spinal cords of IFN-$\gamma^{+/-}$ *H-2*^{q} mice and IFN-$\gamma^{+/+}$ *H-2*^{q} mice, staining of the gray matter was limited to virus antigen scattered among and engulfed by inflammatory cells. Both IFN-$\gamma^{+/+}$ *H-2*^{q} mice (Fig. 8F) and IFN-$\gamma^{-/-}$ *H-2*^{q} mice (Fig. 8H) showed similar virus antigen staining in the spinal cord white matter. Therefore, the expression of IFN-γ had no effect on the expression of virus antigen in the spinal cord white matter in normally susceptible *H-2*^{q} mice. This finding provided strong evidence that the reason for the high morbidity and mortality in IFN-$\gamma^{-/-}$ *H-2*^{q} mice was the prominent infection of motor neurons in the spinal cord.

IFN-γ protects motor neurons from virus-induced death in vitro. To further characterize the neuroprotective effect of IFN-γ, we examined whether spinal motor neurons and the NSC34 spinal motor neuron cell line were protected from DAV-induced cell death in vitro. Previous work had shown that both cultured primary spinal motor neurons and NSC34 cells are killed by DAV and that the 50% effective concentration is 1.5 PFU per cell after 1 day of infection (42). Spinal motor neurons were derived from neonatal B10.D1-H2^q/SgJ mice and cultured for 2 weeks in defined media. Cells were then infected with 1.5 PFU of DAV per cell and incubated overnight in the presence or absence of IFN-γ (100 ng/ml). Cell survival was measured by using an MTT assay as previously described (42). DAV infection resulted in the survival of only 50.5% ± 5.7% ($n = 3$; mean and standard error of the mean; *P* value versus uninfected cells, 0.005) of spinal motor neurons, while concomitant treatment with IFN-γ increased this survival to 78.8% ± 6.9% ($n = 3$; *P* value versus uninfected cells, 0.08; *P* value versus cells only infected with DAV, 0.006) (Fig. 9A). Likewise, DAV infection led to the survival of only 43.7% ± 3.5% ($n = 3$; *P* value versus uninfected cells, 0.0001) of NSC34 cells, and treatment with IFN-γ increased this survival to 62.4% ± 1.1% ($n = 3$; *P* value versus uninfected cells, 0.0003; *P* value versus cells only infected with DAV, 0.007) (Fig. 9A).

We hypothesized that IFN-γ was acting to directly protect spinal motor neurons. To rule out the possibility that IFN-γ was exerting an antiviral effect, we measured VP2 mRNA

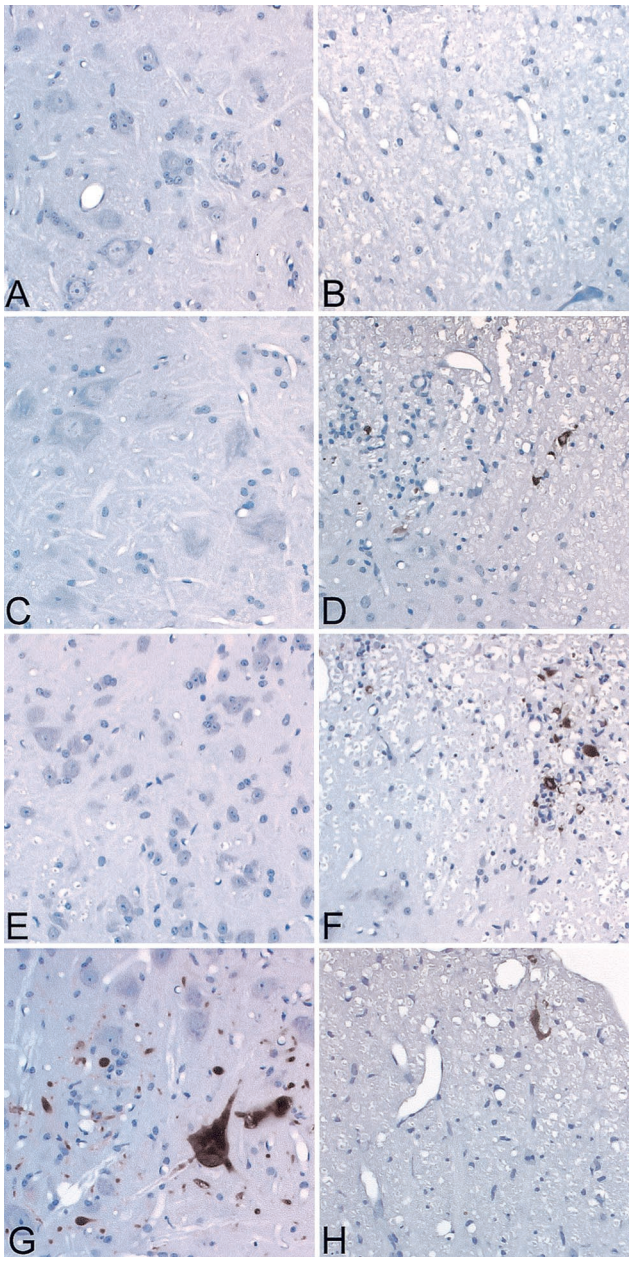

FIG. 8. TMEV infection of gray matter and white matter cells in the spinal cord. Virus antigen staining was performed 16 days after TMEV infection. (A) Absence of virus antigen in anterior horn cells of the spinal cord of an IFN-$\gamma^{+/+}$ *H-2*^{b} mouse (B) Absence of virus antigen in the white matter of an IFN-$\gamma^{+/+}$ *H-2*^{b} mouse. (C) Absence of virus antigen in anterior horn cells of the spinal cord of an IFN-$\gamma^{-/-}$ *H-2*^{b} mouse. (D)Virus antigen in the white matter of an IFN-$\gamma^{-/-}$ *H-2*^{b} mouse. (E) Absence of virus antigen in anterior horn cells of an IFN-$\gamma^{+/+}$ *H-2*^{q} mouse. (F) Presence of virus antigen in the white matter of an IFN-$\gamma^{+/+}$ *H-2*^{q} mouse. (G) Presence of virus antigen in the gray matter of an IFN-$\gamma^{-/-}$ *H-2*^{q} mouse. Virus antigen was localized predominantly in the cytoplasm of neurons. No similar virus antigen-positive anterior horn cell neurons were identified in infected IFN-$\gamma^{+/+}$ *H-2*^{q} or IFN-$\gamma^{+/-}$ *H-2*^{q} mice. (H) Virus antigen localized to the spinal cord white matter of an infected IFN-$\gamma^{-/-}$ *H-2*^{q} mouse.

levels in DAV-infected and IFN-γ-treated NSC34 cells. Using LightCycler real-time PCR analysis, we determined that our detection threshold for VP2 mRNA is 4.14 ± 0.22 $\log_{10}$ copies; values less than or equal to this threshold are indistinguishable from noise. Measurement of VP2 mRNA in uninfected cells revealed 4.85 ± 0.02 $\log_{10}$ viral copies, a value that was not significantly different from the detection threshold ($P = 0.12$) (Fig. 9B). In contrast, we detected 7.13 ± 0.20 $\log_{10}$ viral copies in DAV-infected cells (*P* value versus uninfected cells, 0.0004), and this copy number was unaffected by treatment with IFN-γ (7.25 ± 0.17 $\log_{10}$ viral copies; *P* value verses cells only infected with DAV, 0.67) (Fig. 9B). GAPDH mRNA was also measured in order to verify loading precision and mRNA integrity. As shown in Fig. 9B, GAPDH mRNA levels were the same across all three conditions: we found 5.62 ± 0.18 $\log_{10}$ mRNA copies in uninfected cells, 5.33 ± 0.11 $\log_{10}$ mRNA copies in DAV-infected cells (*P* value versus uninfected cells, 0.24), and 5.40 ± 0.16 $\log_{10}$ mRNA copies in IFN-γ-treated infected cells (*P* value versus uninfected cells, 0.40). Hence, we conclude that IFN-γ did not exert an antiviral influence on cultured motor neurons. We further conclude that the enhanced mortality and pathologic changes observed in IFN-$\gamma^{-/-}$ *H-2*^{q} mice were the result of a deficit in neuroprotection normally afforded by IFN-γ.

DISCUSSION

Our results indicate that IFN-γ is critical for the clearance of virus from anterior horn cell neurons in the spinal cords of susceptible *H-2*^{q} mice following infection with TMEV. Disruption of IFN-γ in normally resistant *H-2*^{b} mice had no effect on early virus-induced injury of neurons. These mice cleared the virus infection normally from the gray matter, likely as a result of a vigorous antiviral class I MHC-restricted cytotoxic lymphocyte response (3, 7). The immunodominant peptide recognized in *H-2*^{b} mice is at amino acids 121 to 130 of VP2 (17). Flow cytometric analysis with VP2 *H-2D*^{b} tetramers indicates that the ratio of VP2-positive CD8 T cells to other types of cells isolated from the brain at 7 days after TMEV infection in IFN-γ-deficient *H-2*^{b} mice is not different from that observed in infected IFN-$\gamma^{+/+}$ *H-2*^{b} mice (16). However, an IFN-γ deficiency in *H-2*^{b} mice did convert these normally resistant mice to mice showing virus persistence in the spinal cord white matter and demyelination after 45 days of TMEV infection. Therefore, IFN-γ in *H-2*^{b} mice protects myelin-roducing oligodendrocytes against persistent infection. Similar results have been observed in the mouse hepatitis virus model of demyelination, where IFN-γ is required for the clearance of virus from CNS oligodendrocytes (40).

In contrast, when we crossed IFN-γ-deficient mice to susceptible *H-2*^{q} mice, the resulting animals showed early death and prominent infection of neurons in the gray matter of the spinal cord. Severe virus-induced injury to anterior horn motor neurons in IFN-$\gamma^{-/-}$ *H-2*^{q} mice is the likely explanation for the clinical phenotype that we observed in *H-2*^{q} mice. *H-2*^{q} mice are susceptible to virus-induced demyelination because they mount a weak or delayed class I MHC-restricted CD8 T-cell response against TMEV (25). In spite of this weak CD8 response to virus, early neuronal infection is cleared in wild-type *H-2*^{q} mice. The presence of virus infection in anterior horn cell

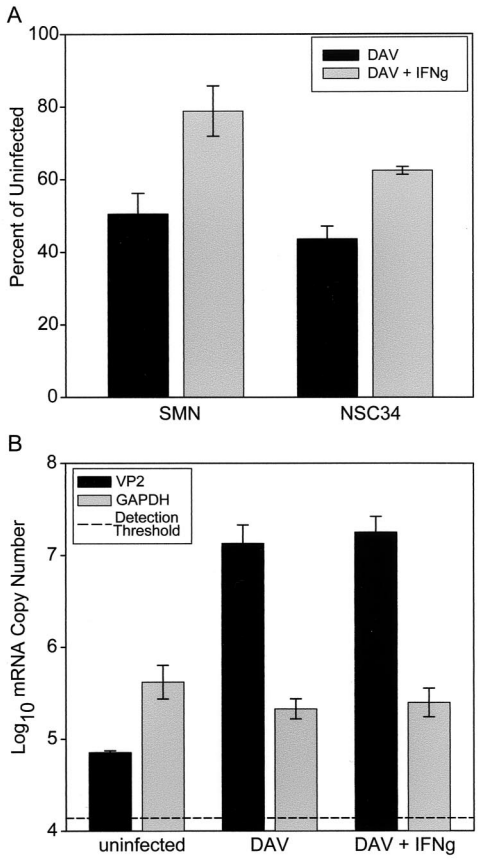

FIG. 9. IFN-γ rescues spinal motor neurons and NSC34 cells from TMEV-induced death. (A) Spinal motor neurons (SMN) or NSC34 cells were infected with 1.5 PFU of DAV per cell and incubated overnight in the presence or absence of 100 ng of IFN-γ/ml. Cell survival was measured by using an MTT assay for metabolically viable cells. Data are expressed as a percentage of the MTT signal measured in uninfected cultures seeded at the same initial cell density. DAV infection resulted in the survival of only 50.5% ± 5.7% ($n = 3$; P value versus uninfected cells, 0.005) of SMN and the survival of only 43.7% ± 3.5% ($n = 3$; P value versus uninfected cells, 0.0001) of NSC34 cells. Treatment with IFN-γ increased the survival of SMN to 78.8% ± 6.9% ($n = 3$; P value versus uninfected cells, 0.08; P value versus cells only infected with DAV, 0.006) and the survival of NSC34 cells to 62.4% ± 1.1% ($n = 3$; P value versus uninfected cells, 0.0003; P value versus cells only infected with DAV, 0.007). (B) In order to rule out an antiviral effect of IFN-γ, VP2 mRNA was quantified by using NSC34 cells infected with 1.5 PFU of DAV per cell and incubated overnight in the presence or absence of IFN-γ (100 ng/ml). The detection threshold for VP2 mRNA established over many experiments was 4.14 ± 0.22 $\log_{10}$ copies. We measured 4.85 ± 0.02 $\log_{10}$ viral copies in uninfected cells (P value versus the detection threshold, 0.12). In contrast, DAV-infected cells contained 7.13 ± 0.20 $\log_{10}$ viral copies (P value versus uninfected cells, 0.0004), and this copy number was unaffected by treatment with IFN-γ (7.25 ± 0.17 $\log_{10}$ viral copies; P value versus cells only infected with DAV, 0.67). GAPDH mRNA was also assessed to control for loading differences: we found 5.62 ± 0.18 $\log_{10}$ mRNA copies in uninfected cells, 5.33 ± 0.11 $\log_{10}$ mRNA copies in DAV-infected cells (P value versus uninfected cells, 0.24), and 5.40 ± 0.16 $\log_{10}$ mRNA copies in IFN-γ-treated infected cells (P value versus uninfected cells, 0.40).

neurons in IFN-$\gamma^{-/-}$ *H-2*^{q} mice indicates that IFN-γ is required for the clearance of virus from neurons in this strain.

Of particular interest is why we saw severe virus infection in spinal cord neurons in IFN-$\gamma^{-/-}$ *H-2*^{q} mice but not in IFN-$\gamma^{-/-}$ *H-2*^{b} mice. This finding would suggest that in the presence of an effective class I MHC-restricted CD8 T-cell response, IFN-γ is not required for the clearance of virus from neurons, whereas when this cytotoxic response is deficient, IFN-γ is critical for neuronal virus clearance or neuronal protection. This notion would imply that in *H-2*^{b} mice, factors other than IFN-γ that are secreted by inflammatory cells are sufficient for neuronal virus clearance. It is possible that direct cytotoxic killing via a perforin-mediated pathway is the mechanism of virus clearance in TMEV-infected *H-2*^{b} mice. However, in *H-2*^{q} mice, where cytotoxic lymphocytes are deficient, IFN-γ secreted by non-CD8 T cells may be required. Using adoptive transfer experiments that resulted in lymphocyte-specific deletion of IFN-γ, Murray et al. showed that IFN-γ secretion by either CD4 or CD8 T cells is independently required for resistance to TMEV disease (35). These experiments demonstrated a greater role in virus clearance for IFN-γ secreted by CD4 T cells than for IFN-γ secreted by CD8 T cells. Murray et al. used bone marrow chimeras to generate mice in which either the hematopoietic cells or the CNS cells lacked the ability to express the IFN-γ receptor and demonstrated that the IFN-γ receptor must be present on CNS glia and not hematopoietic cells to maintain resistance to TMEV infection (35). These results would support the hypothesis that in *H-2*^{q} mice, IFN-γ secreted by CD4 T cells works at the level of CNS glia to limit virus-mediated neuronal injury and viral persistence.

We considered a number of other possibilities to explain the severe spinal cord neuronal infection in IFN-$\gamma^{-/-}$ *H-2*^{q} mice. One possibility is that IFN-γ deficiency affects the antiviral humoral response such that neutralizing antibodies are not generated. We addressed this hypothesis by using a virus-specific ELISA for both IgM and IgG responses in mice of the *H-2*^{q} haplotype with or without the disruption of IFN-γ. Even though IFN-γ might influence the generation of neutralizing antibodies through an indirect effect on the normal activation of helper CD4 T cells (54), no such effect was observed in the virus-specific antibody responses in the ELISA. To explore this possibility further, we examined the neutralization of virus with antiserum from IFN-$\gamma^{-/-}$ *H-2*^{q} or IFN-$\gamma^{+/-}$ *H-2*^{q} mice infected with TMEV for 11 to 16 days. There was no statistical difference in the ability of the serum from either mouse strain to neutralize the virus. Our data indicate that the generation of a neutralizing antibody response to TMEV is independent of IFN-γ in *H-2*^{q} mice.

Another possibility is that IFN-γ deficiency altered the cellular inflammatory response to neuronal infection (35). IFN-γ can activate the release of interleukin 1 and tumor necrosis factor alpha, which augment the function of activated monocytes. These cytokines are part of the acute injury response to foreign antigens and viral infection. In addition, IFN-γ is a potent stimulus for the expression of MHC. To examine this possibility, we evaluated the expression of CD4 T cells, CD8 T cells, F4/80 (macrophages and microglia), class I MHC, and class II MHC in IFN-$\gamma^{-/-}$ *H-2*^{q} mice and IFN-$\gamma^{+/-}$ *H-2*^{q} mice at 12 days after infection. Consistently, we observed less expression of CD4 and CD8 in the spinal cords of IFN-$\gamma^{-/-}$ *H-2*^{q} mice than in those of IFN-$\gamma^{+/-}$ *H-2*^{q} mice. However, the distribution and intensity of F4/80 expression, which identifies microglia and macrophages, were not different between the

mouse strains. In addition, there was a consistent decrease in both class I MHC and class II MHC expression in the spinal cords of infected IFN-$\gamma^{-/-}$ *H-2*^{q} mice compared to IFN-$\gamma^{+/-}$ *H-2*^{q} mice. These observations suggest that the CNS cellular adaptive immune host defense is contingent upon the presence of IFN-γ in *H-2*^{q} mice and that this factor likely contributed to virus persistence in neurons and early deaths in IFN-$\gamma^{-/-}$ *H-2*^{q} mice.

An important possibility is that IFN-γ-deficient mice develop the lethal phenotype following virus infection because of a lack of direct antiviral activity. IFN-γ was initially discovered because of biologic effects on viruses that are similar to those of IFN-β. In vitro replication of vesicular stomatitis virus, poliovirus (type 1), and herpes simplex virus (type 1) is significantly inhibited by IFN-γ-induced type I nitric oxide synthase (19). In contrast, IFN-γ inhibits the replication of influenza virus and Sinbdis virus via a different pathway that does not involve nitric oxide synthase (19). However, in most viral systems, IFN-α/β has a much more pronounced early antiviral effect than IFN-γ. For example, TMEV-infected IFN-α/β receptor-deficient mice develop overwhelming infection of the brain such that even a small amount of input virus results in the death of mice within 2 days of infection (12, 39). These IFN-α/β receptor-deficient mice show massive virus replication, particularly in the hippocampus and striatum. IFN-α has a greater effect than IFN-γ in inhibiting the transmission of herpes virus simplex virus (type 1) from neuronal axons to epidermal cells (32). Since these experiments were done in vitro with a dual-chamber model, the effect of the interferons must be direct, without an influence of the immune response, in the herpes simplex virus model. In addition, in vivo IFN-γ can prevent herpes simplex virus type 1 reactivation from latency in sensory neurons without destroying the infected neurons (30). These experiments support the possibility that IFN-γ can participate in the clearance of infection in neurons without destroying the target.

The final possibility is that IFN-γ works directly to prevent virus-induced death of neurons and thus support the survival of specific neuronal populations. We isolated primary spinal motor neurons from neonatal B10.D1-H2^q/SgJ mice and determined whether IFN-γ could protect these cells from TMEV-induced death without a concomitant antiviral effect. There was clear evidence in the culture model that IFN-γ has a direct effect in preventing anterior horn cell death following virus infection in the absence of an adaptive immune response. This conclusion is further supported by our data from NSC34 motor neurons indicating IFN-γ protects this spinal motor neuron cell line from death induced by infection with TMEV. There is support in the literature for IFN-γ playing a direct role in neuronal survival. For example IFN-γ has been shown to enhance sensory neuron survival that is regulated by suppressor-of-cytokine-signaling proteins (56). Also, CNS-infiltrating T cells may function in neuronal protection to rescue mechanically injured neurons (14). IFN-γ has been shown to be protective of neurons grown in the presence of neurotrophic factors but to be deleterious for cultures deprived of brain-derived neurotrophic factor and neurotrophin-3 (14). In contrast, other investigators (18) have shown conflicting results proposing that IFN-γ induces retrograde dendritic retraction and inhibits synapse formation. We hypothesize that in the TMEV model, IFN-γ functions in vivo to protect anterior horn motor neurons from virus persistence and virus-induced death. Thus, we propose a model in which the release of IFN-γ from T cells exerts a neuroprotective effect that prevents the lethal injury of anterior horn spinal motor neurons following infection with TMEV.

ACKNOWLEDGMENTS

This work was supported by grants P01 NS 38468 and R01 NS 32129 from the National Institutes of Health.

REFERENCES

1. **Altintas, A., Z. Cai, L. R. Pease, and M. Rodriguez.** 1993. Differential expression of H-2K and H-2D in the central nervous system of mice infected with Theiler's virus. J. Immunol. **151:**2803–2812.
2. **Binder, G. K., and D. E. Griffin.** 2001. Interferon-γ-mediated site-specific clearance of alphavirus from CNS neurons. Science **293:**303–306.
3. **Borson, N. D., C. Paul, X. Lin, W. K. Nevala, M. A. Strausbauch, M. Rodriguez, and P. J. Wettstein.** 1997. Brain-infiltrating cytolytic T lymphocytes specific for Theiler's virus recognize *H-2D*^{b} molecules complexed with a viral VP2 peptide lacking a consensus anchor residue. J. Virol. **71:**5244–5250.
4. **Byrnes, A. P., J. E. Durbin, and D. E. Griffin.** 2000. Control of Sindbis virus infection by antibody in interferon-deficient mice. J. Virol. **74:**3905–3908.
5. **Cashman, N. R., H. D. Durham, J. K. Blusztajn, K. Oda, T. Tabira, I. T. Shaw, S. Dahrouge, and J. P. Antel.** 1992. Neuroblastoma x spinal cord (NSC) hybrid cell lines resemble developing motor neurons. Dev. Dyn. **194:**209–221.
6. **Dal Canto, M. C., and H. L. Lipton.** 1982. Ultrastructural immunohistochemical localization of virus in acute and chronic demyelinating Theiler's virus infection. Am. J. Pathol. **106:**20–29.
7. **Dethlefs, S., N. Escriou, M. Brahic, W. S. van der Werf, and E. L. Larsson-Sciard.** 1997. Theiler's virus and Mengo virus induce cross-reactive cytotoxic T lymphocytes restricted to the same immunodominant VP2 epitope in C57BL/6 mice. J. Virol. **71:**5361–5365.
8. **Dethlefs, S., M. Brahic, and E. L. Larsson-Sciard.** 1997. An early, abundant cytotoxic T-lymphocyte response against Theiler's virus is critical for preventing viral persistence. J. Virol. **71:**8875–8878.
9. **Drescher, K. M., C. Rivera-Quinones, C. F. Lucchinetti, and M. Rodriguez.** 1998. Failure of treatment with Linomide or oral myelin tolerization to ameliorate demyelination in a viral model of multiple sclerosis. J. Neuroimmunol. **88:**111–119.
10. **Drescher, K. M., P. D. Murray, C. S. David, L. R. Pease, and M. Rodriguez.** 1999. CNS cell populations are protected from virus-induced pathology by distinct arms of the immune system. Brain Pathol. **9:**21–31.
11. **Egget, C. J., S. Crosier, P. Manning, M. R. Cookson, F. M. Menzies, C. J. McNeil, and P. J. Shaw.** 2000. Development and characterization of a glutamate-sensitive motor neuron cell line. J. Neurochem. **74:**1895–1902.
12. **Fiette, L., C. Aubert, U. Muller, S. Huang, M. Aguet, M. Brahic, et al.** 1995. Theiler's virus infection of 129SV mice that lack the interferon alpha/beta or interferon γ receptors. J. Exp. Med. **181:**2069–2076.
13. **Geiger, K. D., T. C. Nash, S. Sawyer, T. Krahl, G. Patstone, J. C. Reed, S. Krajewski, D. Dalton, M. J. Buchmeier, and N. Sarvetnick.** 1997. Interferon-γ protects against herpes simplex virus type 1-mediated neuronal death. Virology **238:**189–197.
14. **Hammarberg, H., O. Lidman, C. Lundberg, S. Y. Eltayeb, A. W. Gielen, S. Muhallab, A. Svenningsson, H. Linda, P. H. van Der Meide, S. Cullheim, T. Olsson, and F. Piehl.** 2000. Neuroprotection by encephalomyelitis: rescue of mechanically injured neurons and neurotrophin production by CNS-infiltrating T and natural killer cells. J. Neurosci. **20:**5283–5291.
15. **Hasbold, J., J. S. Hong, M. R. Kehry, and P. D. Hodgkin.** 1999. Integrating signals from IFN-γamma and IL-4 by B cells: positive and negative effects on CD40 ligand-induced proliferation, survival, and division-linked isotype switching to IgG1, IgE, and IgG2a. J. Immunol. **163:**4175–4181.
16. **Johnson, A. J., M. K. Njenga, M. J. Hansen, S. T. Kuhns, L. Chen, M. Rodriguez, and L. R. Pease.** 1999. Prevalent class I-restricted T-cell response to the Theiler's virus epitope *D*^{b}*:VP2*$_{121–130}$ in the absence of endogenous CD4 help, tumor necrosis factor alpha, gamma interferon, perforin, or costimulation through CD28. J. Virol. **73:**3702–3708.
17. **Johnson, A. J., J. Upshaw, K. D. Pavelko, M. Rodriguez, and L. R. Pease.** 2001. Preservation of motor function by inhibition of CD8+ virus peptide-specific T cells in Theiler's virus infection. FASEB J. **15:**2760–2762.
18. **Kim, I. J., H. N. Beck, P. J. Lein, and D. Higgins.** 2002. Interferon γ induces retrograde dendritic retraction and inhibits synapse formation. J. Neurosci. **22:**4530–4539.
19. **Komatsu, T., Z. Bi, and C. S. Reiss.** 1996. Interferon-γ induced type I nitric oxide synthase activity inhibits viral replication in neurons. J. Neuroimmunol. **68:**101–108.

20. **Koustova, E., Y. Sei, T. McCarty, M. G. Espey, R. Ming, H. C. Morse III, and A. S. Basile.** 2000. Accelerated development of neurochemical and behavioral deficits in LP-BM5 infected mice with targeted deletions of the IFN-gamma gene. J. Neuroimmunol. **108:**112–121.
21. **Levine, B., J. M. Hardwick, B. D. Trapp, T. O. Crawford, R. C. Bollinger, and D. E. Griffin.** 1991. Antibody-mediated clearance of alphavirus infection from neurons. Science **254:**856–860.
22. **Levy, M., C. Aubert, and M. Brahic.** 1992. Theiler's virus replication in brain macrophages cultured in vitro. J. Virol. **66:**3188–3193.
23. **Lin, X., N. R. Thiemann, L. R. Pease, and M. Rodriguez.** 1995. VP1 and VP2 capsid proteins of Theiler's virus are targets of H-2D-restricted cytotoxic lymphocytes in the central nervous system of B10 mice. Virology **214:**91–99.
24. **Lin, X., L. R. Pease, and M. Rodriguez.** 1997. Differential generation of class I H-2D- versus H-2K-restricted cytotoxicity against a demyelinating virus following central nervous system infection. Eur. J. Immunol. **27:**963–970.
25. **Lin, X., L. R. Pease, and M. Rodriguez.** 1998. Theiler's virus infection of genetically susceptible mice induces CNS-infiltrating cytotoxic T lymphocytes without apparent viral or major myelin antigenic specificity. J. Immunol. **160:**5661–5668.
26. **Lindsley, M. D., A. K. Patick, N. Prayoonwiwat, and M. Rodriguez.** 1992. Coexpression of class I major histocompatibility antigen and viral RNA in central nervous system of mice infected with Theiler's virus: a model for multiple sclerosis. Mayo Clin. Proc. **67:**829–838.
27. **Lindsley, M. D., and M. Rodriguez.** 1989. Characterization of the inflammatory response in the central nervous system of mice susceptible or resistant to demyelination by Theiler's virus. J. Immunol. **142:**2677–2682.
28. **Lindsley, M. D., R. Thiemann, and M. Rodriguez.** 1991. Cytotoxic T cells isolated from the central nervous systems of mice infected with Theiler's virus. J. Virol. **65:**6612–6620.
29. **Lipton, H. L.** 1975. Theiler's virus infection in mice: an unusual biphasic disease process leading to demyelination. Infect. Immun. **11:**1147–1155.
30. **Liu, T., K. M. Khanna, B. N. Carriere, and R. L. Hendricks.** 2001. Gamma interferon can prevent herpes simplex virus type 1 reactivation from latency in sensory neurons. J. Virol. **75:**11178–11184.
31. **Medana, I., M. A. Martinic, H. Wekerle, and H. Neumann.** 2001. Transection of major histocompatibility complex class I-induced neurites by cytotoxic T lymphocytes. Am. J. Pathol. **159:**809–815.
32. **Mikloska, Z., and A. L. Cunningham.** 2001. Alpha and gamma interferons inhibit herpes simplex virus type 1 infection and spread in epidermal cells after axonal transmission. J. Virol. **75:**11821–11826.
33. **Munoz-Fernandez, M. A., and M. Fresno.** 1998. The role of tumour necrosis factor, interleukin 6, interferon-γ and inducible nitric oxide synthase in the development and pathology of the nervous system. Prog. Neurobiol. **56:**307–340.
34. **Murphy, K. M., W. Ouyang, J. D. Farrar, J. Yang, S. Ranganath, H. Asnagli, M. Afkarian, and T. L. Murphy.** 2000. Signaling and transcription in T helper development. Annu. Rev. Immunol. **18:**451–494.
35. **Murray, P. D., D. B. McGavern, L. R. Pease, and M. Rodriguez.** 2002. Cellular sources and targets of IFNγ-mediated protection against viral demyelination and neurologic deficits. Eur. J. Immunol. **32:**606–615.
36. **Neumann, H.** 2001. Control of glial immune function by neurons. Glia **36:**191–199.
37. **Njenga, M. K., K. D. Pavelko, J. Baisch, X. Lin, C. David, J. Leibowitz, and M. Rodriguez.** 1996. Theiler's virus persistence and demyelination in major histocompatibility complex class II-deficient mice. J. Virol. **70:**1729–1737.
38. **Njenga, M. K., K. Asakura, S. F. Hunter, P. Wettstein, L. R. Pease, and M. Rodriguez.** 1997. The immune system preferentially clears Theiler's virus from the gray matter of the central nervous system. J. Virol. **71:**8592–8601.
39. **Njenga, M. K., L. R. Pease, P. Wettstein, T. Mak, and M. Rodriguez.** 1997. Interferon α/β mediates early virus-induced expression of H-2D and H-2K in the central nervous system. Lab. Investig. **77:**71–84.
40. **Parra, B., D. R. Hinton, N. W. Marten, C. C. Bergmann, M. T. Lin, C. S. Yang, and S. A. Stohlman.** 1999. IFN-γamma is required for viral clearance from central nervous system oligodendroglia. J. Immunol. **162:**1641–1647.
41. **Patterson, C. E., D. M. Lawrence, L. A. Echols, and G. F. Rall.** 2002. Immune-mediated protection from measles virus-induced central nervous system disease is noncytolytic and gamma interferon dependent. J. Virol. **76:**4497–4506.
42. **Pavelko, K. D., C. L. Howe, K. M. Drescher, J. D. Gamez, A. J. Johnson, T. Wei, R. M. Ransohoff, and M. Rodriguez.** 2003 Related. Interleukin-6 protects anterior horn neurons from lethal virus-induced injury. J. Neurosci. **23:**481–492.
43. **Pierce, M. L., and M. Rodriguez.** 1989. Erichrome stain for myelin on osmicated tissue embedded in glycol methacrylate plastic. J. Histotechnol. **12:**35–36.
44. **Rodriguez, M., J. L. Leibowitz, and P. W. Lampert.** 1983. Persistent infection of oligodendrocytes in Theiler's virus-induced encephalomyelitis. Ann. Neurol. **13:**426–433.
45. **Rodriguez, M., and C. S. David.** 1985. Demyelination induced by Theiler's virus: influence of the H-2 haplotype. J. Immunol. **135:**2145–2148.
46. **Rodriguez, M., W. P. Lafuse, J. Leibowitz, and C. S. David.** 1986. Partial suppression of Theiler's virus-induced demyelination in vivo by administration of monoclonal antibodies to immune-response gene products (Ia antigens). Neurology **36:**964–970.
47. **Rodriguez, M., J. Leibowitz, and C. S. David.** 1986. Susceptibility to Theiler's virus-induced demyelination. Mapping of the gene within the H-2D region. J. Exp. Med. **163:**620–631.
48. **Rodriguez, M., M. D. Lindsley, and M. L. Pierce.** 1991. Role of T cells in resistance to Theiler's virus infection. Microb. Pathog. **11:**269–281.
49. **Rodriguez, M., C. Nickerson, A. K. Patick, and C. S. David.** 1991. Expression of human HLA-B27 transgene alters susceptibility to murine Theiler's virus-induced demyelination. J. Immunol. **146:**2596–2602.
50. **Rodriguez, M., A. J. Dunkel, R. L. Thiemann, J. Leibowitz, M. Zijlstra, and R. Jaenisch.** 1993. Abrogation of resistance to Theiler's virus-induced demyelination in H-2b mice deficient in beta 2-microglobulin. J. Immunol. **151:**266–276.
51. **Rodriguez, M., R. P. Roos, D. McGavern, L. Zoecklein, K. Pavelko, H. Sang, and X. Lin.** 2000. The CD4-mediated immune response is critical in determining the outcome of infection using Theiler's viruses with VP1 capsid protein point mutations. Virology **275:**9–19.
52. **Rossi, C. P., M. Delcroix, I. Huitinga, A. McAllister, N. van Rooijen, E. Claassen, and M. Brahic.** 1997. Role of macrophages during Theiler's virus infection. J. Virol. **71:**3336–3340.
53. **Sidman, R. L., J. B. Angevine, and E. T. Pierce.** 1971. Atlas of the mouse brain and spinal cord, p. 6. Harvard University Press, Cambridge, Mass.
54. **Snapper, C. M., and W. E. Paul.** 1987. Interferon-γ and B-cell stimulatory factor-1 reciprocally regulate Ig isotype production. Science **236:**944–947.
55. **Trottier, M., P. Kallio, W. Wang, and H. L. Lipton.** 2001. High numbers of viral RNA copies in the central nervous system of mice during persistent infection with Theiler's virus. J. Virol. **75:**7420–7428.
56. **Turnley, A. M., R. Starr, and P. F. Bartlett.** 2001. SOCS1 regulates interferon-γ mediated sensory neuron survival. NeuroReport **12:**3443–3445.